

## METALLICITY VARIATIONS IN THE TYPE II GLOBULAR CLUSTER NGC 6934\*

A. F. MARINO,<sup>1</sup> D. YONG,<sup>1</sup> A. P. MILONE,<sup>2</sup> G. PIOTTO,<sup>2</sup> M. LUNDQUIST,<sup>3</sup> L. R. BEDIN,<sup>4</sup> A.-N. CHENÉ,<sup>3</sup> G. DA COSTA,<sup>1</sup>  
M. ASPLUND,<sup>1</sup> AND H. JERJEN<sup>1</sup>

<sup>1</sup>*Research School of Astronomy & Astrophysics, Australian National University, Canberra, ACT 2611, Australia*

<sup>2</sup>*Dipartimento di Fisica e Astronomia “Galileo Galilei” - Univ. di Padova, Vicolo dell’Osservatorio 3, Padova, IT-35122*

<sup>3</sup>*Gemini Observatory, Northern Operations Centre, 670 North A’ohoku Place, Hilo, HI 96720, USA*

<sup>4</sup>*Istituto Nazionale di Astrofisica - Osservatorio Astronomico di Padova, Vicolo dell’Osservatorio 5, Padova, IT-35122*

Submitted to ApJ

### ABSTRACT

The *Hubble Space Telescope* photometric survey of Galactic globular clusters (GCs) has revealed a peculiar “chromosome map” for NGC 6934. Besides a typical sequence, similar to that observed in Type I GCs, NGC 6934 displays additional stars on the red side, analogous to the *anomalous*, Type II GCs, as defined in our previous work. We present a chemical abundance analysis of four red giants in this GC. Two stars are located on the chromosome map sequence common to all GCs, and another two on the additional sequence. We find: (i) star-to-star Fe variations, with the two *anomalous* stars being enriched by  $\sim 0.2$  dex. Due to our small-size sample, this difference is at the  $\sim 2.5 \sigma$  level; (ii) no evidence for variations in the *slow* neutron-capture abundances over Fe, at odds with what is often observed in *anomalous* Type II GCs, e.g. M 22 and  $\omega$  Centauri; (iii) no large variations in light elements C, O and Na, compatible with the targets location on the lower part of the chromosome map where such variations are not expected. Since the analyzed stars are homogeneous in light elements, the only way to reproduce the photometric splits on the sub-giant (SGB) and the red-giant (RGB) branches is to assume that red-RGB/faint-SGB stars are enhanced in  $[\text{Fe}/\text{H}]$  by  $\sim 0.2$ . This fact corroborates the spectroscopic evidence of a metallicity variation in NGC 6934. The observed chemical pattern resembles only partially the other Type II GCs, suggesting that NGC 6934 might belong either to a third class of GCs, or be a link between *normal* Type I and *anomalous* Type II GCs.

*Keywords:* globular clusters: individual (NGC 6934) — chemical abundances – Population II – Hertzsprung-Russell diagram

### 1. INTRODUCTION

In the last few years there have been an increasing number of observations that indicate a sizeable sub-sample of the Milky Way globular clusters (GCs) host stellar populations with different metallicities (here intended as primarily Fe). These variations are in addition to the typical star-to-star variations observed for elements involved in hot-H burning processes, e.g. C, N, O, Na, and sometimes Mg, and Al.

The *Hubble Space Telescope* (*HST*) UV-Legacy of Galactic GCs (Piotto et al. 2015) has recently revealed that the multiple stellar populations phenomenon in GCs is best described by the so-called “chromosome map”, a diagram constructed from a combination of *HST* filters whose  $x$  ( $\Delta_{\text{F275W},\text{F814W}}$ ) and  $y$  ( $\Delta_{\text{C F275W},\text{F336W},\text{F438W}}$ ) axes are mostly sensitive to helium and nitrogen, respectively (Milone et al. 2015, 2017). These diagrams were given their name because they represent a imprint of the formation processes that occurred in GCs which produced what we

Corresponding author: A. F. Marino  
[anna.marino@anu.edu.au](mailto:anna.marino@anu.edu.au)

\* Based on observations with the NASA/ESA *Hubble Space Telescope*, obtained at the Space Telescope Science Institute, which is operated by AURA, Inc., under NASA contract NAS 5-26555. This paper includes data gathered with the 6.5 meter Magellan Telescopes located at Las Campanas Observatory, Chile, and Gemini Telescope at Canada-France-Hawaii Telescope.

observe today as multiple stellar populations. The morphology of the chromosome maps varies from cluster to cluster, displaying different extensions and numbers of overdensities, corresponding to different stellar populations.

Despite some degree of variation between the maps, common features have been observed (Renzini et al. 2015; Milone et al. 2017). First, stars in all the GCs display a common pattern in their chromosome map extending from relatively low  $\Delta_C$  F275W,F336W,F438W and high  $\Delta_{F275W,F814W}$  values, to lower  $\Delta_{F275W,F814W}$  and higher  $\Delta_C$  F275W,F336W,F438W. Second, a first stellar generation (1G), defined by the population of stars located at the lower  $\Delta_C$  F275W,F336W,F438W values of the map, has been identified in all GCs investigated so far. Stars associated with the second generation (2G) are found at higher  $\Delta_C$  F275W,F336W,F438W defining a sequence in both  $\Delta_{F275W,F814W}$  and  $\Delta_C$  F275W,F336W,F438W, that extends from lower- $\Delta_C$  F275W,F336W,F438W/higher- $\Delta_{F275W,F814W}$ , towards different degrees of enhanced  $\Delta_C$  F275W,F336W,F438W values. As these feature have been observed as a general behavior in Milky Way GCs, the GCs showing exclusively these features have been named Type I GCs (Milone et al. 2017).

However, ten of the 57 GCs in the *HST* study have photometric peculiarities (Milone et al. 2017). These objects, named Type II GCs, in addition to the common 1G and 2G stars observed in Type I GCs, display additional sequences in the red side of their chromosome map. These red stars usually follow the same pattern observed for the 1G and 2G stars in Type-I GCs, i.e. a distribution from high- $\Delta_{F275W,F814W}$ /low- $\Delta_C$  F275W,F336W,F438W to lower- $\Delta_{F275W,F814W}$ /higher- $\Delta_C$  F275W,F336W,F438W. However, the lowest  $\Delta_C$  F275W,F336W,F438W values observed for the red stars changes from cluster to cluster.

All the Type II GCs for which chemical abundances are available from spectroscopy have been classified as *anomalous* GCs, i.e. as GCs exhibiting internal variations not just in the light elements involved in hot-H burning processes, but also in the bulk metallicity and in heavier elements, specifically in elements produced via *slow* neutron-capture reactions ( $[s\text{-elements}/\text{Fe}]$ ). Type II GCs include NGC 1851 (Yong & Grundahl 2008), M 22 (Marino et al. 2009, 2011; Lee 2016), NGC 5286 (Marino et al. 2015), M 2 (Yong et al. 2014), and, the most extreme case,  $\omega$  Centauri (e.g. Norris & Da Costa 1995; Johnson & Pilachowski 2010; Marino et al. 2011). In all cases variations in  $[s\text{-elements}/\text{Fe}]$  are positively correlated with Fe. Further, in NGC 1851 (Yong et al. 2009, 2015), M 22 (Marino et al. 2011) and  $\omega$  Centauri (Marino et al. 2012) a difference in the overall C+N+O abundance has been found, with the stars enriched in  $[s\text{-elements}/\text{Fe}]$  also having higher  $[\text{C+N+O}/\text{Fe}]$  abundances. As stellar populations with different C+N+O are expected to have distinct luminosities on the sub-giant branch (SGB), these chemical variations are considered to play an important role in generating the split SGBs observed in these three GCs (Milone et al. 2008; Cassisi et al. 2008; Marino et al. 2012a,b).

The complex chemical pattern of *anomalous* clusters and its resemblance on a less extreme scale to  $\omega$  Centauri have raised the intriguing idea that these GCs could have originated in extra-Galactic environments (Bekki & Freeman 2003). Specifically, these GCs could be the surviving nuclei of now-disrupted dwarf galaxies, similar to what has been proposed to explain the chemical variations in  $\omega$  Centauri. Such a dwarf galaxy environment could explain the capability of these GCs to support more extended star formation histories than typical GCs which show variations in light elements only.

In this context, M 54 stands out as an intriguing case (Carretta et al. 2010). It is the nuclear star cluster of the Sagittarius dwarf galaxy (Bellazzini et al. 2008) and certainly formed and evolved in an extra-Galactic environment. The photometric and spectroscopic similarities between M 54 and the other *anomalous* GCs, makes it tempting to speculate that the latter are indeed remnants of dwarf galaxies cannibalized by the Milky Way.

To date heavy elements variations have been observed in 11 Galactic GCs. Most surprisingly, the *HST* UV Survey has revealed that a relatively large fraction of the total sample of the 57 observed clusters,  $\sim 18\%$ , belongs to the class of Type II GCs. We don't know yet if all Type II GCs can also be classified as *anomalous* from their chemistry, but all the *anomalous* GCs behave as Type II, based on their chromosome maps. The idea that such a large fraction of GCs ( $\sim 18\%$ ) could be chemically *anomalous* would mean that many GCs in the Milky Way had a deeper potential well with which to retain high velocity supernovae ejecta required to explain metallicity variations, and possibly be dwarf galaxy remnants.

In the present study we continue our investigation of Type II GC properties. For that purpose, we focus on the chemical abundances of a poorly studied GC, NGC 6934, which exhibits an unusual chromosome map. This metal-intermediate cluster ( $[\text{Fe}/\text{H}] = -1.47$ , Harris 1996, as updated in 2010) has been classified as a Type II GC since it hosts a split SGB visible in the optical filters which is connected with a red red-giant branch (RGB) that is absent in typical Milky Way GCs (Milone et al. 2017). On the other hand, the position of these red RGB stars is slightly different from what is observed in *anomalous* GCs, as they lie at lower average  $\Delta_C$  F275W,F336W,F438W values. Proper motions suggest that the *red* sequence stars on the chromosome map are cluster members, but they have never been

investigated for chemical abundances. To better understand the chemical properties of multiple stellar populations in NGC 6934 we have selected four targets, two in each of the two sequences identified in its chromosome map.

The outline of the paper is as follows: Section 2 is a description of the spectroscopic and photometric data-sets; the choice of the adopted atmospheric parameters is discussed in Section 3, while our chemical abundance analysis is outlined in Section 4. Section 5 describes the results, which are summarized and discussed in Section 6.

## 2. DATA

### 2.1. The photometric dataset: the chromosome map of NGC 6934

The photometric data used in this study come from the *HST* UV Legacy Survey which investigated multiple stellar populations in GCs (GO-13297, Piotto et al. 2015). Details on the images analyzed and on the data reduction can be found in Piotto et al. (2015) and Milone et al. (2017). Photometry has been corrected for differential reddening effects, which are very small,  $\Delta(E(B - V)) \lesssim 0.004$  mag, for NGC 6934.

Milone et al. (2017) analyzed the chromosome map of 57 GCs, including NGC 6934, and noticed some peculiarities (see their Fig. 4) for this cluster with respect to typical GCs maps. The chromosome map of NGC 6934 red giants is reproduced on the left panel of Fig. 1, with the dashed line separating 2G from 1G stars as defined in Milone et al. (2017). In this parameter space we can clearly distinguish: (i) the presence of 1G and 2G stars, as the stars located below and above the dashed line, respectively; and (ii) two distinct patterns of stars represented with gray and red dots, respectively. The presence of the separate distribution of red stars on the chromosome map is a distinctive feature of the Type II GCs.

Another distinctive feature of Type II GCs is the presence of a split SGB in both optical and UV color-magnitude diagrams (CMDs). As shown in the right panel of Fig. 1, the faint SGB of NGC 6934 is clearly connected with the red RGB in the  $m_{F336W}$  vs.  $m_{F336W} - m_{F814W}$  CMD. Red stars on the chromosome map have been selected as the stars defining the red RGB on the CMD, represented in the right panel of Fig. 1.

From its optical and ultraviolet CMDs and from its chromosome map, NGC 6934 has been classified as a Type II GC, though, as discussed in Section 1, the comparison of the chromosome map of NGC 6934 with that observed in *anomalous* GCs suggests that the majority of *red* stars in *anomalous* GCs have higher values on the  $\Delta_{C\ F275W, F336W, F438W}$  axis. This difference in the distribution of the stars can be easily seen in Fig. 2 where we represent the chromosome map of NGC 6934 (left panel) in comparison with that of the *anomalous* GC M22 (middle panel). For comparison purposes, we also display the chromosome map of the Type I GC NGC 6752 (right panel), which exhibits the presence of just 1G and 2G stars. In all the three GCs shown in Fig. 2, the dashed line represents the separation between 1G and 2G stars, as defined in Milone et al. (2017). It is clear that while in M22 all the red stars have  $\Delta_{C\ F275W, F336W, F438W}$  values above the 1G-2G separation line, some red stars in NGC 6934 lie below this line.

To avoid confusion, we repeat here the terminology that will be used throughout the paper. Firstly, according to their chemical compositions, GCs are classified into *normal* and *anomalous* (e.g. Marino et al. 2015). Following this classification, in this paper the terms *normal* and *anomalous* will refer to the chemical pattern observed in GCs from spectroscopy:

- *normal* are the monometallic systems with the typical chemical patterns observed in GCs, e.g. the (anti-) correlations in light elements;
- *anomalous* will indicate GCs with unusual chemical pattern in heavy elements, e.g. variations in the [*s*-element/Fe] ratios and/or [Fe/H];

Secondly, according to their photometric pattern (Milone et al. 2017), GCs will be identified as:

- Type I, which will be used for GCs with single SGBs in CMDs from photometry with optical filters. These objects display the typical chromosome map characterised by a *single* sequence;
- Type II, which designates those GCs with a split SGB in optical filter CMDs. These clusters exhibit a blue and red RGB in the  $m_{F336W}$  vs.  $m_{F336W} - m_{F814W}$  CMD. Stars on red RGB also define additional red sequences on the chromosome map.

The synergy between photometry and spectroscopy reveals that: (i) *normal* GCs exhibit the CMDs and the chromosome maps of Type I GCs; (ii) all the *anomalous* GCs analyzed so far are Type II and the stars with enhanced Fe and/or [*s*-element/Fe] populate the red RGB. In the following we will also refer to individual stars in Type II GCs as:

- blue- or *normal* RGB stars if they define the blue RGB and fall in the typical chromosome map sequence, as observed in all GCs;
- red- or *anomalous* RGB stars if they are located on the additional red sequences, observed in Type II GCs only;
- in this paper the targets on the *normal* and *anomalous* RGBs will be designated n1, n2 and a1, a2, respectively.

## 2.2. The spectroscopic dataset

Our spectroscopic data have been acquired using the Gemini Remote Access to CFHT ESPaDOnS (Donati 2003) Spectrograph (GRACES; Chené et al. 2014) through the program GN-2015B-Q-81, and with the Magellan Inamori Kyocera Echelle (MIKE, Bernstein et al. 2003) spectrograph on the Magellan-Clay 6.5m telescope. The targets were four RGB stars with  $V \sim 15$  mag selected from the chromosome map described in Section 2.1. Their location in the chromosome map and in the  $m_{F336W} - (m_{F336W} - m_{F814W})$  CMD of NGC 6934 are shown in Fig. 1. We have chosen two giants lying on the *normal* RGB and two on the *anomalous* RGB, represented with blue filled circles and red stars, respectively. As our primary goal is to study the heavy element pattern, we note here that our spectroscopic sample are biased towards relatively low values of  $\Delta_C F_{275W, F336W, F438W}$ . This choice was made to avoid contamination from stars characterised by substantially different abundances of nitrogen and/or other light elements (Milone et al. 2017). Furthermore, our selected targets are among the brightest 1G stars in order to maximize the S/N of the spectra. The observing log is given in Tab. 1.

High resolution ( $R \sim 40,000$ ) optical spectra were obtained with GRACES in August and December 2015 using the target+sky 2-fibre spectroscopic mode. Briefly, light from the Gemini North telescope is fed to the Echelle SpectroPolarimetric Device for the Observation of Stars (ESPaDOnS) at the Canada-France-Hawaii Telescope (CFHT) via two 270 m long optical fibres which have  $\sim 8$  per cent throughput (see Chené et al. 2014). Basic data reduction was performed using the OPERA pipeline (Martioli et al. 2012, Malo et al., in preparation). Two of the four targets observed with GRACES, were subsequently re-observed with MIKE with the aim of gathering independent analysis from a different data set. Specifically, we gathered MIKE spectra for one target on the *normal* sequence, and one on the *anomalous* sequence, chosen to have very similar effective temperatures based on the analysis of the GRACES data. The MIKE spectra were taken in 2017 May, using a  $0.70''$  slit which gives  $R \sim 35,000$  in the blue and  $R \sim 30,000$  in the red, respectively. Data reduction involving bias-subtraction, flat-field correction, wavelength-calibration, and sky-subtraction, has been done by using the dedicated CarPy pipeline<sup>1</sup> (Kelson et al. 2000; Kelson 2003).

Both for the GRACES and MIKE spectra, co-addition of the individual exposures, continuum normalisation, radial velocity (RV) determination and correction to laboratory wavelength was performed using IRAF routines. Spectral coverage for the GRACES spectra is  $\sim 4070$ - $10020 \text{ \AA}$ , while the MIKE spectra cover the spectral region from  $\sim 3350 \text{ \AA}$  to  $\sim 9420 \text{ \AA}$ . The S/N ratio of our MIKE spectra is  $\sim 120@6000 \text{ \AA}$ , while the GRACES spectra have a lower S/N, between 40 and  $70@6000 \text{ \AA}$ . The chemical abundance analysis was performed by neglecting the bluest part of the spectra because of the low S/N. Specifically, we have analysed the spectral regions with  $\lambda \gtrsim 4200 \text{ \AA}$  for MIKE, and  $\lambda \gtrsim 4500 \text{ \AA}$  for GRACES.

Radial velocities were derived using the IRAF@FXCOR task, which cross-correlates the object spectrum with a template. For the template we used a synthetic spectrum generated with the latest version of MOOG<sup>2</sup> (Snedden 1973). This spectrum was computed with a model stellar atmosphere interpolated from the Kurucz (1992) grid<sup>3</sup>, adopting parameters (effective temperature ( $T_{\text{eff}}$ ), surface gravity ( $\log g$ ), microturbulent velocity ( $\xi_t$ ), and overall metallicity ( $[A/H]$ ) of 4600 K, 2.5,  $2.0 \text{ km s}^{-1}$ , and  $-1.45$  dex, respectively. Observed RVs were then corrected to the heliocentric system.

Heliocentric RVs were used as a proof of cluster membership for our targets. We measure an average RV for the four stars of  $\langle RV \rangle = -405.5 \pm 2.9 \text{ km s}^{-1}$  (rms=  $5.0 \text{ km s}^{-1}$ ), which is consistent with the Harris tabulated value of  $-411.4 \pm 1.6 \text{ km s}^{-1}$  (Harris 2010). Such extreme negative RVs are clearly distinct from the RVs of typical field stars. Hence, based on both RVs and proper motions, we can be confident of the membership for all four targets. Coordinates and RVs, both observed (RV) and corrected to the heliocentric system ( $RV_{\text{helio}}$ ), for all four stars are listed in Tab. 1.

<sup>1</sup> See <http://code.obs.carnegiescience.edu/mike>

<sup>2</sup> <http://www.as.utexas.edu/chris/moog.html>.

<sup>3</sup> <http://kurucz.harvard.edu/grids.html>

### 3. MODEL ATMOSPHERES

The relatively high resolution and the large spectral coverage of our spectra allowed us to have a fully-spectroscopic estimate of the stellar parameters,  $T_{\text{eff}}$ ,  $\log g$ ,  $[\text{A}/\text{H}]$  and  $\xi_t$ . Hence, we determined  $T_{\text{eff}}$  by imposing the excitation potential (E.P.) equilibrium of the Fe I lines and gravity with the ionization equilibrium between Fe I and Fe II lines. Note that for  $\log g$  we impose Fe II abundances that are 0.05-0.07 dex higher than the Fe I ones to adjust for non-local thermodynamic equilibrium (non-LTE) effects (Bergemann et al. 2012; Lind, Bergemann & Asplund 2012). For this analysis,  $\xi_t$  was set to minimize any dependence of Fe I abundances as a function of EW. For the two stars observed with both GRACES and MIKE, we derived the atmospheric parameters separately for each spectrum.

As an independent test of our results, we also derived atmospheric parameters from our *HST* photometry (see Section 2.1). The  $m_{\text{F606W}}$  and  $m_{\text{F814W}}$  mag have been converted to  $V$  and  $I$  mag (Anderson et al. 2008), which we then used to estimate temperatures from the Alonso et al. (1999) color-temperature calibrations. The use of the  $(V - I)$  color for this purpose is justified by the fact that it is mostly insensitive to variations in light elements. Surface gravities were then obtained from the apparent  $V$  magnitudes, the photometric  $T_{\text{eff}}$ , bolometric corrections from Alonso et al. (1999), apparent distance modulus of  $(m - M)_V = 16.28$  (Harris 2010), and masses of  $0.80 M_{\odot}$ . Once  $T_{\text{eff}}$  and  $\log g$  have been fixed from photometry, we derived  $\xi_t$  from the Fe I lines as explained above. The atmospheric parameters obtained from spectroscopy and photometry are listed in Tab. 2.

By comparing the spectroscopic stellar parameters obtained from the GRACES and MIKE spectra for the two stars observed with both instruments we notice that: (i) GRACES  $T_{\text{eff}}$  are only marginally higher; (ii)  $\log g$  values agree within  $\lesssim 0.20$  dex; (iii) GRACES metallicities are systematically higher by  $\sim 0.20$  dex. By adopting exactly the same atmospheric parameters from photometry (right columns in Tab. 2) for the MIKE and GRACES spectra, we have a mean difference in  $[\text{Fe}/\text{H}]$  of 0.135 dex between stars observed with both the instruments, with higher values for GRACES. We have verified that this difference is introduced by the systematically higher EWs, by  $\sim 6$  mÅ, obtained from the GRACES spectra. We note here that the MIKE Fe abundances are in better accord with the tabulated Harris value ( $[\text{Fe}/\text{H}] = -1.47$  dex; Harris 2010). As abundance offsets are not unexpected when using spectra from different spectrographs, in the following we will consider results from different instruments separately, and average them appropriately only when necessary.

We adopt as our primary set of atmospheric parameters the values obtained from the MIKE spectra, as they have higher S/N and a larger number of measured Fe lines. For GRACES, due to the low number of measurable lines, in particular Fe II, we prefer to adopt the parameters based on photometry as our primary set. In the following, when appropriate, we will use both the sets of parameters to check our results.

In order to have an estimate of the internal errors associated with our atmospheric parameters, we have compared our  $T_{\text{eff}}/\log g$  values from the spectral lines with those derived from the  $(V - I)$  *HST* colors. We obtain:  $\Delta T_{\text{eff}} = T_{\text{eff, Fe lines}} - T_{\text{eff}(V-I)} = +126 \pm 21$  K (rms=48 K), and  $\Delta \log g = \log g_{\text{Fe lines}} - \log g_{(V-I)} = +0.06 \pm 0.06$  (rms=0.14). This comparison suggests that the spectroscopic  $T_{\text{eff}}/\log g$  scales are systematically higher, but the internal errors in these parameters are smaller, comparable with the rms of the average differences, e.g. about 50 K and 0.15 dex, in temperature and gravity, respectively. Furthermore, in our chemical abundance analysis we adopt typical internal uncertainties of  $0.20 \text{ km s}^{-1}$  for  $\xi_t$  and 0.10 dex for metallicity.

### 4. CHEMICAL ABUNDANCES ANALYSIS

Chemical abundances were derived from a LTE analysis by using the spectral analysis code MOOG (Sneden 1973), and the alpha-enhanced Kurucz model atmospheres of Castelli & Kurucz (2004), whose parameters have been obtained as described in Section 3.

A list of our analyzed spectral lines, with their associated equivalent widths (EWs), excitation potentials (EPs) and total oscillator strengths ( $\log gf$ ), is provided in Tab. 2. The chemical abundances for all the elements, with the exception of those discussed below, have been inferred from an EW-based analysis. We now comment on some of the transitions that we used.

*Proton-capture elements:* We have derived abundance ratios with respect to Fe for C, O, Na, Al and Mg. Carbon has been inferred from spectral synthesis of the CH G-band ( $A^2\Delta - X^2\Pi$ ) features near 4312 and 4323 Å. The S/N of the GRACES spectra at these wavelengths was too low to derive abundances, so C has been measured only from MIKE spectra. Oxygen abundances were inferred from the synthesis of the forbidden [O I] lines at 6300 Å and 6363 Å. Although we have not derived any 3D-non-LTE correction for these spectral lines, we notice that from the grid by Amarsi et al. (2016) that they are small for metal-poor stars within their analysed range of atmospheric parameters

( $5000 < T_{\text{eff}} < 6500$  K,  $3.0 < \log g < 5.0$  g/cm s<sup>-2</sup>). Our giants are, however, somewhat cooler, and have much lower surface gravities. Further, telluric O<sub>2</sub> and H<sub>2</sub>O spectral absorptions often affect the O line at 6300 Å. Indeed, for our targets, the analyzed O transition is contaminated by O<sub>2</sub> lines. We have removed the telluric features by using the software MOLECFIT<sup>4</sup> provided by ESO (Smette et al. 2014; Kausch et al. 2014). Nevertheless, even with such a subtraction procedure, we caution that residual telluric feature contamination might be of concern for the analysis of the 6300.3 [O I] line. We determined Na abundances from the EWs of the Na I doublets at  $\sim 5680$  Å,  $\sim 6150$  Å and  $\sim 8190$  Å. Chemical abundances for this species have been corrected for non-LTE effects by following the recipes in Lind et al. (2011). Aluminum was inferred from the synthesis of the doublet at  $\sim 6667$  Å, while magnesium abundances were determined from the EWs of the transitions at  $\sim 5528$ , 5711 Å.

*Manganese:* For Mn, we have synthesised the spectral lines at around 4710, 4739, 4754, 4762, 5395, 5420, 5433, 6014, 6022 Å, by assuming  $f(^{55}\text{Mn})=1.00$ . When available, the hyperfine splitting data have been taken from Lawler et al. (2001a,b), otherwise from the Kurucz (2009) compendium<sup>5</sup>.

*Copper:* Abundances for Cu were inferred from synthesis of the Cu I lines at 5105, 5782 Å. Both hyperfine and isotopic splitting were included in the analysis, using the well-studied spectral line component structure from Kurucz (2009). Solar-system isotopic fractions were assumed in the computations:  $f(^{63}\text{Cu})=0.69$  and  $f(^{65}\text{Cu})=0.31$ .

*Neutron-capture elements:* We derived Sr, Y, Zr, Ba, La, Ce, Pr, Nd, Sm, Eu and Dy abundances from the MIKE spectra, and Y, Ba, La, Ce, Pr, Nd, Sm, Eu from the GRACES spectra. For all these elements we performed a spectral synthesis analysis, as hyperfine and/or isotopic splitting and/or blending features needed to be taken into account. In all the cases we have assumed the Solar-system isotopic fractions.

The inferred chemical abundances are listed in Tabs. 4–5. Internal uncertainties in chemical abundances due to the adopted model atmospheres were estimated by varying the stellar parameters, one at a time, by the amounts derived in Section 3, namely  $T_{\text{eff}}/\log g/[\text{Fe}/\text{H}]/\xi_t = \pm 50$  K/ $\pm 0.15$  cgs/ $\pm 0.10$  dex/ $\pm 0.20$  km s<sup>-1</sup>. Another way to evaluate how the adopted model atmospheres affect our results is by comparing chemical abundances for the same stars inferred from the spectroscopic and photometric parameters. This test is particularly enlightening since we have adopted spectroscopic parameters for MIKE data and photometric parameters for GRACES. In the lower panel of Fig. 3 we plot the differences  $\Delta[\text{X}/\text{Fe}]$  between the chemical abundances obtained from the photometric and the spectroscopic parameters for the stars n2 and a2 (observed with both MIKE and GRACES) for the elements available from both the data sets. We note that the differences are generally small, of the order of a few hundredth dex, and, in any case, lower than 0.10 dex<sup>6</sup>. The upper panel represents the differences between the chemical abundances obtained from GRACES (photometric parameters) and MIKE (spectroscopic parameters) spectra for the stars n2 and a2. Here the differences are larger, up to  $\sim 0.20$  dex. The arrows displays the amount and direction of the variation in each species due to the different sets of atmospheric parameters. We note that, even if in a few cases, e.g. Si, the set of atmospheric parameters can explain the differences in the inferred abundances, in most cases the distinct results have simply to be ascribed to the different data sets and to the different spectral lines used in the analysis.

In addition to the contribution introduced by internal errors in atmospheric parameters, we estimated the contribution due to the limits of our spectra, e.g. due to the finite S/N that affects the measurements of EWs and the spectral synthesis. For MIKE spectra, the uncertainty in the EWs measurements has been estimated to be  $\pm 4.4$  mÅ by comparing the observed distribution of the differences between the Fe lines' EWs for the two MIKE stars and the corresponding distribution expected from simulated spectra (see Section 5.1). For GRACES spectra we have compared the EWs obtained from individual exposures of the same stars and obtained typical errors in EWs of 5 mÅ and 7 mÅ for the two *normal* and the two *anomalous* stars (the latter having lower S/N), respectively. For each spectrum, the errors in chemical abundances due to the EWs have been calculated by varying the EWs of spectral lines by the corresponding uncertainty. For the species inferred from spectral synthesis we have varied the continuum at the  $\pm 1 \sigma$  level, and re-derived the chemical abundances from each line. Since the EWs/continuum placement errors are random, the error associated to those elements with a larger number of lines is lower. Hence, the corresponding uncertainty associated with Fe I is negligible (0.01 dex), while for those species inferred from one or two spectral lines, the error due to the limited S/N is dominant (e.g. Al, or Ce and Pr for GRACES spectra). All the error estimates are listed in Tab. 5 for both the MIKE spectra and the GRACES spectra, separately in the latter case for the normal and anomalous stars.

<sup>4</sup> <http://www.eso.org/sci/software/pipelines/skytools/molecfit>

<sup>5</sup> Available at: <http://kurucz.harvard.edu/>

<sup>6</sup> Iron is not included in this plot because we treat it separately in Section 5.1

## 5. THE CHEMICAL COMPOSITION OF NGC 6934

The mean metallicity obtained from our stars in NGC 6934 is  $[\text{Fe}/\text{H}] = -1.44 \pm 0.13$  dex (rms=0.13 dex) from the two MIKE stars (spectroscopic parameters), and  $[\text{Fe}/\text{H}] = -1.37 \pm 0.12$  dex (rms=0.12 dex) from the four stars observed with GRACES (photometric parameters). Figure 4 shows a summary of the other chemical abundance ratios obtained for the two stars analyzed with MIKE (upper panel), and for the four stars analyzed with GRACES (lower panels).

As is typical for Population II, the NGC 6934 stars are  $\alpha$ -enhanced. More specifically, the chemical abundances relative to Fe for the stars on the *normal* and *anomalous* RGB are the same within the observational errors for all element groups, i.e.  $\alpha$ , light, Fe-peak, and  $n$ -capture elements. In the next few subsections we consider and discuss all the interesting abundance patterns we observe in NGC 6934, focusing on those elements which play an important role in the multiple stellar populations phenomenon. We start with iron, and then discuss the  $p$ -capture elements and finally the  $n$ -process elements.

## 5.1. Iron abundances

Even though our sample of stars is small, the results immediately suggest the presence of Fe internal variations in NGC 6934. From a simple comparison between the spectra of the *normal* and *anomalous* stars n2 and a2, which have very similar atmospheric parameters, it is clear that a2 displays stronger lines, as shown in Fig. 5. On the other hand, the hydrogen lines ( $\text{H}\alpha$  and  $\text{H}\beta$ ) are very similar, confirming that the stars have the same effective temperature.

Figure 6 displays the Fe I and Fe II abundances as a function of  $\Delta_{\text{F275W},\text{F814W}}$  for the analyzed stars, for both the MIKE and GRACES spectra. We note the systematic higher Fe abundances for the GRACES data, as discussed in Section 3, but to avoid these systematic differences in our discussion, we will refer to the relative Fe differences observed in each data set, separately.

In particular, the iron abundances, both neutral and singly ionized, are higher in the stars located on the *anomalous* RGB. This remains valid independent of which set of atmospheric parameters are used, spectroscopic or photometric. These *anomalous* stars also have higher  $\Delta_{\text{F275W},\text{F814W}}$  values than *normal* RGB stars in the chromosome map.

In all the panels, two error bars have been associated with each Fe measurement: the error defined as  $\text{r.m.s.}/\sqrt{(N-1)}$ , where  $N$  is the number of lines (gray error bars); and the expected error due to the model atmospheres and the S/N (black error bars, as discussed in Section 4). The larger number of available Fe I lines (upper panels) translates in a statistical error  $\text{r.m.s.}/\sqrt{(N-1)}$  smaller than the one associated with Fe II (lower panels). The expected errors listed in Tab. 2 are larger, ranging between 0.09 to 0.11 for Fe I, and between 0.12 to 0.18 for Fe II.

Quantitatively, we obtain  $\Delta[\text{Fe I}/\text{H}] = 0.18 \pm 0.13$  dex for MIKE (by construction  $\Delta[\text{Fe II}/\text{H}]$  is the same, but has a larger error of  $\pm 0.16$ ); and  $\Delta[\text{Fe I}/\text{H}] = 0.21 \pm 0.15$  dex,  $\Delta[\text{Fe II}/\text{H}] = 0.23 \pm 0.18$  dex, for GRACES. The weighted averages of the two *normal* and *anomalous* stars observed with GRACES are  $\langle[\text{Fe I}/\text{H}]\rangle = -1.47 \pm 0.08$  dex and  $\langle[\text{Fe II}/\text{H}]\rangle = -1.26 \pm 0.07$  dex, respectively which means  $\Delta[\text{Fe I}/\text{H}] = 0.21 \pm 0.11$  dex. By taking advantage of the measurements from both MIKE and GRACES, the weighted  $\Delta[\text{Fe I}/\text{H}]$  mean value is  $\Delta[\text{Fe I}/\text{H}] = 0.20 \pm 0.08$  dex, which is a significance of  $\sim 2.5 \sigma$ .

Although the small observed sample prevents us from drawing strong conclusions on the higher Fe abundance for the *anomalous* RGB stars, the Fe enrichment is observed in all our available measurements, independent of the set of the adopted stellar parameters and/or data. Thus, it is very tempting to conclude that the *anomalous* stars are enriched in the overall metallicity. In the following we present a few independent tests to corroborate the presence of Fe variations in NGC 6934.

First, in Fig. 7 we show the difference in EWs for the Fe lines between the two stars observed with MIKE (a2–n2). The observed differences have been compared with those expected for two simulated spectra with the same atmospheric parameters of the two target stars. We note that, while the observed mean difference for Fe I is relatively high, 9.9 mÅ, that for the Fe II is smaller, 2.9 mÅ. In both cases the observed differences agree well with those expected from theoretical spectra ( $\Delta\text{EWs}(\text{Fe I}) = 10.4$  mÅ and  $\Delta\text{EWs}(\text{Fe II}) = 1.2$  mÅ). The small difference in the Fe II lines is well explained by the atmospheric parameters of our stars. Indeed, we get higher surface gravities for the two stars located on the chromosome map's *anomalous* sequence. And, assuming that all the other atmospheric parameters are identical, a star with higher  $\log g$  is expected to show smaller EWs.

Second, an independent test that provides further evidence for iron variations in NGC 6934 comes from the comparison between the observed CMD and stellar isochrones. Figure 8 represents the  $m_{\text{F336W}} - (m_{\text{F336W}} - m_{\text{F814W}})$  and  $m_{\text{F438W}} - (m_{\text{F438W}} - m_{\text{F606W}})$  CMDs for the cluster. The presence of an additional sequence, on the red side of the main RGB, is clear in the  $m_{\text{F336W}} - (m_{\text{F336W}} - m_{\text{F814W}})$  CMD. Stars in the *anomalous* RGB, which *evolve* from a fainter

SGB, correspond to the stars defining the *anomalous* sequence on the chromosome map (on Fig. 1), and are also located redder in the  $m_{F438W}-(m_{F438W} - m_{F606W})$  CMD. Superimposed on both CMDs are isochrones corresponding to an age=12.25 Gyr,  $Y=0.2471$ ,  $[\alpha/Fe]=+0.40$  and  $[Fe/H]=-1.40$  (dark red) and  $[Fe/H]=-1.60$  (black), retrieved from the Dartmouth database (Dotter et al. 2008). Although the upper part of the RGB is poorly represented by these isochrones, especially in the  $m_{F336W}-(m_{F336W} - m_{F814W})$  CMD (possibly due to the contribution of CNO abundances to  $m_{F336W}$ ), the fit on the lower RGB and the SGB is satisfactory, with only some systematic shift of both isochrones on the RGB blue side. We conclude that a difference in  $[Fe/H]$  by  $\sim 0.2$  dex can reproduce the CMD of NGC 6934. According to our *HST* high-precision CMD, NGC 6934 hosts one main stellar population, and one minor component that is slightly enriched in Fe, and which constitutes  $7\pm 1\%$  of the cluster mass (Milone et al. 2017).

The inset in Fig. 8, shows the theoretical  $\log g$ - $T_{\text{eff}}$  plane from the Dartmouth isochrones with  $[Fe/H]=-1.60$  and  $[Fe/H]=-1.40$ . Superimposed are our adopted atmospheric parameters for the analysed stars, specifically spectroscopic parameters for MIKE and photometric parameters for GRACES (see Section 3). Both sets of adopted  $\log g$ - $T_{\text{eff}}$  parameters agree with the parameters expected from theoretical isochrones and satisfy the basic principle that at a given  $T_{\text{eff}}$  stars with higher metallicity have higher  $\log g$ . Specifically, the  $\log g$  difference expected at  $T_{\text{eff}}\sim 4450$  K is  $\sim 0.15$ - $0.20$  dex, consistent with our estimates.

### 5.2. Light elements

The abundance ratios obtained for the *p*-capture elements from C to Al have been plotted in the left panel of Fig. 9. As a comparison, we have also included the same elements derived for M 22 by Marino et al. (2009, 2011). A first fact to note is that the analyzed stars in NGC 6934 do not seem to show large dispersions in these elements. All our NGC 6934 targets lie in the O-rich/Na-Al-poor range, e.g. they all share a primordial chemical composition as regards the *p*-capture elements. On the other hand, both the *s*-poor and the *s*-rich stars analysed in M 22 span a relatively large range of abundances in all these elements, including stars with chemical composition typical for second-generation(s), e.g. O-depleted and Na-Al-enhanced. Carbon abundances have been inferred only for the two stars observed with MIKE, and the *normal* and the *anomalous* stars show similar values.

The lack of second-generation(s) stars in our NGC 6934 sample is due to the selection of our targets, which is biased towards stars located in the lower part of the chromosome map with relatively low  $\Delta_C F_{275W,F336W,F438W}$  values. As shown in Milone et al. (2017), first population stars possess relatively low values of  $\Delta_C F_{275W,F336W,F438W}$ , and relatively high values of  $\Delta_{F275W,F814W}$ . The choice to observe only stars in the lower part of the chromosome map is justified by our goal to investigate any difference (if present) between the chemical composition of stars in the *normal* and *anomalous* RGBs. To do this, we tried to avoid additional effects such as the variation in light elements within the *normal* and *anomalous* categories. We expect that second population(s) stars, with low O and high Na, would be observed to have higher  $\Delta_C F_{275W,F336W,F438W}$  values. In this context, the higher Na and Al abundance ratios inferred for the *normal* star n1 agree with its position on the chromosome map, given its slightly higher  $\Delta_C F_{275W,F336W,F438W}$ . Future observations will enlighten the light elements distribution in the *normal* and *anomalous* RGBs of NGC 6934.

### 5.3. *s*-process elements

On the right panel of Fig. 9 we show the abundance ratios of some of the analyzed *n*-capture elements, specifically Y, Ba, La and Nd relative to Fe, as a function of  $[Fe/H]$  both from MIKE and GRACES spectra. As done for the light elements, in each panel we plot the corresponding results obtained for M 22 (data from Marino et al. 2009; 2011).

Although it is a more metal poor GC, M 22 has been chosen for comparison purposes because it shows a clear bimodality in *n*-capture elements. Typically, in *anomalous* GCs, like M 22, the variation in *n*-capture elements is due to additional *s*-process enrichment among some second generation stars (Marino et al. 2011). Specifically, M 22 hosts a stellar population relatively enriched in the *s*-process elements (*s*-rich group) with respect to a stellar population with lower *s*-elements abundance ratios (*s*-poor group). The *s*-rich group is also enhanced in Fe by  $\sim 0.15$  dex and in the overall  $[C+N+O/Fe]$  (Marino et al. 2009, 2011, 2012). However, the *n*-capture element  $[Eu/Fe]$  ratio, which is mostly produced via *rapid* neutron capture reactions (*r*-process element), is uniform.

We note that the difference in Fe between the *s*-rich and the *s*-poor groups of M 22 is similar to the measured difference between the *normal* and *anomalous* stars in NGC 6934. However, while for M 22 the variation in Fe is coupled with a variation in  $[s\text{-elements}/Fe]$ , with the Fe-richer stars displaying higher  $[s\text{-elements}/Fe]$ , the analyzed stars in NGC 6934 exhibit similar content for Y, Ba, La, and Nd relative to Fe. Indeed, by considering, e.g. La, which is one of the *s*-elements with more precise measured abundances, we derive a difference of  $|\Delta[La/Fe]| = 0.05\pm 0.11$  dex



(from MIKE data) and  $|\Delta[\text{La}/\text{Fe}]| = -0.10 \pm 0.11$  dex (from GRACES data), compared to the significantly larger difference  $|\Delta[\text{La}/\text{Fe}]| = 0.32 \pm 0.02$  dex between the *s*-rich and *s*-poor group of M 22. We recall here that M 22 displays one of the smallest internal variation in the  $[\text{s-element}/\text{Fe}]$  ratio among the known *anomalous* GCs (see e.g. Fig. 19 in Marino et al. 2015). For comparison, M 2 has  $|\Delta[\text{La}/\text{Fe}]| = 0.58$  dex (Yong et al. 2014), NGC 5286  $|\Delta[\text{La}/\text{Fe}]| = 0.56$  dex (Marino et al. 2015), and NGC 6273  $|\Delta[\text{La}/\text{Fe}]| = 0.42$  dex (Johnson et al. 2017).

Clearly, the Type II GC NGC 6934 seems different from the chemically-defined class of *anomalous* GCs, as our analysed sample does not show any evidence of additional internal variations in *s*-elements. This conclusion is based only on four stars, and future observations on larger sample sizes may perhaps reveal the presence of stars enhanced in *s*-elements located in other regions of the chromosome map. On the other hand, we note that, despite our sample of only four stars, they have been carefully selected from the two different sequences in the chromosome map where we expect variations in heavy elements, as observed in the *anomalous* GCs. Photometrically, *s*-rich stars in *anomalous* GCs are located on the red RGB (Milone et al. 2017). We cannot exclude, however, a different behavior for NGC 6934.

An inspection of the other *n*-capture species in Fig. 4 (from Sr to Dy for MIKE and from Y to Eu for GRACES) clearly suggests the lack of any significant internal variation in the analysed elements in NGC 6934. In this figure we note a growth of the abundances relative to Fe as a function of the atomic number in both the *normal* and *anomalous* stars.

## 6. DISCUSSION AND CONCLUSIONS

We have presented a high-resolution chemical abundance analysis of four stars on the *normal* and *anomalous* RGB of NGC 6934. We have found that the chemical abundances of all the inferred species, except Fe, are consistent with uniform abundance ratios in the four analyzed stars. The difference in Fe is of the order of  $\sim 0.2$  dex with two *anomalous* RGB stars exhibiting higher abundances. Such variation in Fe is corroborated by the comparison between the CMDs obtained from high-precision *HST* photometry and the isochrones of Dotter et al. (2008).

NGC 6934 has been classified as a Type II GC as, contrary to Type I GCs, it displays more than the normal 1G and 2G sequences in the  $\Delta_{\text{F}275\text{W},\text{F}814\text{W}} - \Delta_{\text{C F}275\text{W},\text{F}336\text{W},\text{F}438\text{W}}$  photometric plane. Milone et al. (2017) have shown that the *main* pattern on the chromosome map in all GCs, both Type I and Type II, corresponds to a distribution in light element abundances: stars with different He, C, N, O, and Na abundances distribute from higher  $\Delta_{\text{F}275\text{W},\text{F}814\text{W}}$  and lower  $\Delta_{\text{C F}275\text{W},\text{F}336\text{W},\text{F}438\text{W}}$  to lower  $\Delta_{\text{F}275\text{W},\text{F}814\text{W}}$  and higher  $\Delta_{\text{C F}275\text{W},\text{F}336\text{W},\text{F}438\text{W}}$ .

The presence of numerous additional sequences on the red side of the main chromosome map appears in  $\sim 18\%$  of the analyzed GCs (Type II). For a subsample of these GCs, it was possible to identify some stars with available chemical abundances along the sequences of the chromosome map, and it appeared that the additional red sequences are populated by stars enriched in both Fe and *s*-elements relative to Fe (*anomalous* GCs). This behavior is observed also in  $\omega$  Centauri.

For simplicity, a list of the currently known chemically *anomalous* and/or photometrically peculiar Type II GCs is provided in Tab. 7. In the light of the new findings coming from the synergy between spectroscopic and photometric investigation, we propose a slightly different and simpler terminology to define this new class of GCs, as listed in the last column of the table:

- Iron II are the objects with variations in Fe, in contrast to the typical GCs, designated Iron I, that do not show evidence for star-to-star variations in Fe;
- *s* II is used for the GCs with variations in *s*-elements, while typical GCs are labeled *s*-I;
- following Milone et al. (2017), Type II is used for the GCs with additional red sequences on the chromosome map, while typical GCs are Type I.

By using this terminology, NGC 6934 can be classified as a Iron II/*s*-I/Type II GC. However, we cannot exclude that a future analysis of larger sample sizes may reveal stars with enhancements in the *s*-elements.

Our results show that, although NGC 6934 is classified as a Type II GC, its *anomalous* stars do not exhibit any enrichment in the *s*-process elements relative to Fe, although variations in the  $[\text{Fe}/\text{H}]$  abundances are present. At present, NGC 6934 is the only Type II GC with available spectroscopy on the *red* sequence of the chromosome map,

that displays chemical variations in Fe, but not in the  $s$ -elements<sup>7</sup>. A larger sample of stars would help to assess if the Fe distribution in NGC 6934 is continuous or consistent with two discrete populations.

Another photometric similarity between NGC 6934 and *anomalous* GCs with chemical variations in  $[s\text{-elements/Fe}]$  is the split SGB, as shown in Figs. 1 and 8. In the *anomalous* GCs this feature has been associated with the presence of stellar populations with different C+N+O (Marino et al. 2011; 2012). As an example, the comparison between isochrones and the CMD of M22, reveals that a variation in Fe alone could not reproduce the observed SGB split (Marino et al. 2009). In contrast, isochrones with the same age and with a metallicity difference of 0.2 dex, corresponding to the observed Fe difference between the *normal* and *anomalous* stars, can account for the size of the SGB split in NGC 6934, without invoking any variation in the overall C+N+O. Although we cannot estimate the total C+N+O for NGC 6934 without N abundance measurement, the lack of additional internal variations in  $s$ -process elements points to no strong intra-cluster pollution by low-mass asymptotic giant branch stars that underwent third dredge-up (at least not at the level observed in the  $s$  II GCs); and might in turn suggests no variations in the  $[C+N+O/Fe]$  (e.g. Karakas 2010).

We emphasize here that the shape of the distribution of the *anomalous-red* stars in the chromosome map of NGC 6934 shows a few differences from that observed in other *anomalous* GCs. While, most of the *red* stars in the *anomalous* GCs, such as M 22, have relatively high values of  $\Delta_C F_{275W, F336W, F438W}$ , suggesting an enrichment in light elements, in NGC 6934 they are located on the lower part of the diagram (see Fig. 2). Even though we think it is very unlikely to have  $s$ -enriched stars at higher  $\Delta_C F_{275W, F336W, F438W}$  with a lack of them at lower values, we cannot exclude it *a priori*. Future observations sampling a larger number of stars on all the stellar populations appearing in the chromosome map of NGC 6934 will allow us to better constrain the extent of the Fe variations in this GC.

Our chemical abundance analysis suggests that there is no one-to-one correlation between the appearance of *red* additional sequences on the chromosome maps of Type II GCs and variations in  $s$ -elements and, possibly C+N+O. Could these sequences, instead, be more directly linked to enrichments in the overall metallicity? This idea opens a new perspective in the interpretation of the origin of  $\sim 18\%$  of the Milky Way GCs. Could all these objects have been significantly more massive than typical GCs in order to support a more prolonged star formation? Could the retention of SNe ejecta hint that these objects originated in a deeper potential well, such as the nucleus of a dwarf galaxy (Da Costa 2015)? Future observations will shed light on the answers to these questions.

The authors thank the anonymous referee for useful discussion.

Australian access to the Magellan Telescopes was supported through the National Collaborative Research Infrastructure Strategy of the Australian Federal Government.

Based on observations obtained with ESPaDOnS, located at the Canada-France-Hawaii Telescope (CFHT). CFHT is operated by the National Research Council of Canada, the Institut National des Sciences de l'Univers of the Centre National de la Recherche Scientifique of France, and the University of Hawai'i. ESPaDOnS is a collaborative project funded by France (CNRS, MENESR, OMP, LATT), Canada (NSERC), CFHT and ESA. ESPaDOnS was remotely controlled from the Gemini Observatory, which is operated by the Association of Universities for Research in Astronomy, Inc., under a cooperative agreement with the NSF on behalf of the Gemini partnership: the National Science Foundation (United States), the National Research Council (Canada), CONICYT (Chile), Ministerio de Ciencia, Tecnología e Innovación Productiva (Argentina) and Ministério da Ciência, Tecnologia e Inovação (Brazil).

AFM, GDC and HJ acknowledge support by the Australian Research Council through Discovery Early Career Researcher Award DE160100851 and Discovery projects DP150103294 and DP150100862. APM has been supported by the European Research Council through the Starting Grant "GALFOR".

*Facilities:* Magellan:Clay, Gemini:Gillett, HST

## REFERENCES

Alonso, A., Arribas, S., & Martínez-Roger, C. 1999, A&AS,

<sup>7</sup> Yong et al. (2014) has shown that the extremely Fe-rich population in M22, contrary to the Fe-intermediate one, does not show any enhancement in the  $[s\text{-elements/Fe}]$ . However the extremely Fe-rich stars have other chemical peculiarities, such as lower  $[Ca/Fe]$  abundances.

Alves-Brito, A., Yong, D., Meléndez, J., Vásquez, S., &

Karakas, A. I. 2012, A&A, 540, A3

- Amarsi, A. M., Asplund, M., Collet, R., & Leenaarts, J. 2016, *MNRAS*, 455, 3735
- Anderson, J., Sarajedini, A., Bedin, L. R., et al. 2008, *AJ*, 135, 2055
- Bekki, K., & Freeman, K. C. 2003, *MNRAS*, 346, L11
- Bellazzini, M., Ibata, R. A., Chapman, S. C., et al. 2008, *AJ*, 136, 1147
- Bergemann, M., Lind, K., Collet, R., Magic, Z., & Asplund, M. 2012, *MNRAS*, 427, 27
- Bernstein, R., Shtetman, S. A., Gunnels, S. M., Mochnecki, S., & Athey, A. E. 2003, *SPIE*, 4841, 1694
- Brown, J. A., Wallerstein, G., & Gonzalez, G. 1999, *AJ*, 118, 1245
- Carretta, E., Bragaglia, A., Gratton, R. G., et al. 2010, *ApJL*, 714, L7
- Carretta, E., Bragaglia, A., Gratton, R. G., et al. 2013, *A&A*, 557, A138
- Cassisi, S., Salaris, M., Pietrinferni, A., et al. 2008, *ApJL*, 672, L115
- Castelli, F., & Kurucz, R. L. 2004, arXiv:astro-ph/0405087
- Chené, A.-N., Padzer, J., Barrick, G., et al. 2014, *SPIE*, 9151, 915147
- Da Costa, G. S., Held, E. V., Saviane, I., & Gullieuszik, M. 2009, *ApJ*, 705, 1481
- Da Costa, G. S., Held, E. V., & Saviane, I. 2014, *MNRAS*, 438, 3507
- Da Costa, G. S. 2015, *IAU General Assembly*, 22, 2249201
- D’Orazi, V., Gratton, R. G., Pancino, E., et al. 2011, *A&A*, 534, A29
- Dotter, A., Chaboyer, B., Jevremović, D., et al. 2008, *ApJS*, 178, 89-101
- Ferraro, F. R., Dalessandro, E., Mucciarelli, A., et al. 2009, *Nature*, 462, 483
- Gratton, R. G., Lucatello, S., Sollima, A., et al. 2013, *A&A*, 549, AA41
- Harris, W. E. 1996, *AJ*, 112, 1487
- Harris, W. E. 2010, arXiv:1012.3224
- Johnson, C. I., & Pilachowski, C. A. 2010, *ApJ*, 722, 1373
- Johnson, C. I., Rich, R. M., Pilachowski, C. A., et al. 2015, *AJ*, 150, 63
- Johnson, C. I., Caldwell, N., Rich, R. M., et al. 2017, *ApJ*, 836, 168
- Karakas, A. I. 2010, *MNRAS*, 403, 1413
- Kausch, W., Noll, S., Smette, A., et al. 2014, *Astronomical Society of the Pacific Conference Series*, 485, 403
- Kelson, D. D., Illingworth, G. D., van Dokkum, P. G., & Franx, M. 2000, *ApJ*, 531, 159
- Kelson, D. D. 2003, *PASP*, 115, 688
- Kurucz, R. L. 2009, *American Institute of Physics Conference Series*, 1171, 43
- Lardo, C., Pancino, E., Mucciarelli, A., et al. 2013, *MNRAS*, 433, 1941
- Lawler, J. E., Bonvallet, G., & Sneden, C. 2001a, *ApJ*, 556, 452
- Lawler, J. E., Wickliffe, M. E., den Hartog, E. A., & Sneden, C. 2001b, *ApJ*, 563, 1075
- Lee, J.-W. 2016, *ApJS*, 226, 16
- Lind, K., Asplund, M., Barklem, P. S., & Belyaev, A. K. 2011, *A&A*, 528, A103
- Lind, K., Bergemann, M., & Asplund, M. 2012, *MNRAS*, 427, 50
- Marino, A. F., Milone, A. P., Piotto, G., et al. 2009, *A&A*, 505, 1099
- Marino, A. F., Sneden, C., Kraft, R. P., et al. 2011a, *A&A*, 532, A8
- Marino, A. F., Milone, A. P., Piotto, G., et al. 2011b, *ApJ*, 731, 64
- Marino, A. F., Milone, A. P., Sneden, C., et al. 2012a, *A&A*, 541, A15
- Marino, A. F., Milone, A. P., Piotto, G., et al. 2012b, *ApJ*, 746, 14
- Marino, A. F., Milone, A. P., Yong, D., et al. 2014, *MNRAS*, 442, 3044
- Marino, A. F., Milone, A. P., Karakas, A. I., et al. 2015, *MNRAS*, 450, 815
- Martoli, E., Teeple, D., Manset, N., et al. 2012, *SPIE*, 8451, 84512B
- Massari, D., Mucciarelli, A., Ferraro, F. R., et al. 2014, *ApJ*, 795, 22
- Milone, A. P., Bedin, L. R., Piotto, G., et al. 2008, *ApJ*, 673, 241-250
- Milone, A. P., Marino, A. F., Piotto, G., et al. 2015, *MNRAS*, 447, 927
- Milone, A. P., Piotto, G., Renzini, A., et al. 2017, *MNRAS*, 464, 3636
- Norris, J. E., & Da Costa, G. S. 1995, *ApJ*, 447, 680
- Norris, J. E., Freeman, K. C., & Mighell, K. J. 1996, *ApJ*, 462, 241
- Origlia, L., Rich, R. M., Ferraro, F. R., et al. 2011, *ApJL*, 726, L20
- Piotto, G., Milone, A. P., Bedin, L. R., et al. 2015, *AJ*, 149, 91
- Renzini, A., D’Antona, F., Cassisi, S., et al. 2015, *MNRAS*, 454, 4197
- Roederer, I. U., Mateo, M., Bailey, J. I., et al. 2016, *MNRAS*, 455, 2417
- Smette, A., et al. 2014, submitted
- Smith, V. V., Suntzeff, N. B., Cunha, K., et al. 2000, *AJ*, 119, 1239
- Sneden, C. 1973, *ApJ*, 184, 839

Suntzeff, N. B., & Kraft, R. P. 1996, *AJ*, 111, 1913

Villanova, S., Geisler, D., & Piotto, G. 2010, *ApJL*, 722, L18

Yong, D., & Grundahl, F. 2008, *ApJL*, 672, L29

Yong, D., Grundahl, F., D'Antona, F., et al. 2009, *ApJL*, 695, L62

Yong, D., Roederer, I. U., Grundahl, F., et al. 2014, *MNRAS*, 441, 3396

Yong, D., Grundahl, F., & Norris, J. E. 2015, *MNRAS*, 446, 3319

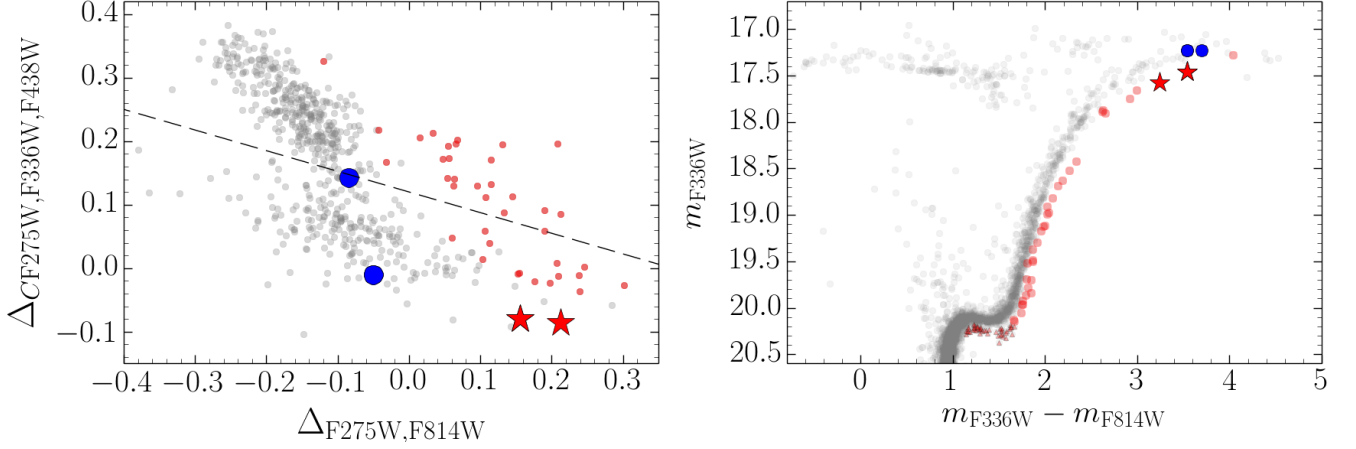


**Figure 1.** Location of the spectroscopic targets in the chromosome map (left panel) and the  $m_{F336W}$  vs.  $(m_{F336W} - m_{F814W})$  CMD (right panel) of NGC 6934. The stars coloured in red on the chromosome map have been selected as the stars defining the redder RGB stars on the CMD in the right panel (red circles). Gray symbols represent *normal* RGB stars, which are observed in both Type I and Type II GCs. The red triangles on the CMD represent the faint SGB stars of NGC 6934. The dashed black line on the map is the same as used in Milone et al. (2017) to separate 2G from 1G stars. Spectroscopic targets located on the *normal* and *anomalous* RGBs are shown as blue circles and red star-like symbols, respectively.

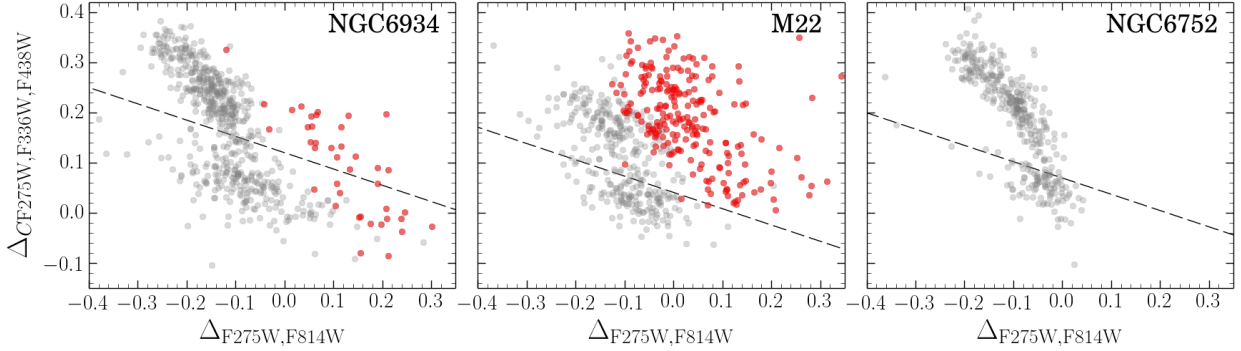


**Figure 2.** Comparison between the chromosome map of RGB stars in the Type I GC NGC 6752 (right panel) and in the Type II GCs NGC 6934 (left) and M 22 (middle). We colored gray the stars in the *normal* RGB, which are observed in both Type I and Type II GCs. Type II GCs exhibit an additional sequence of *anomalous* RGB stars, which are colored in red. In all the panels, the dashed black line separates 2G from 1G stars, as in Milone et al. (2017).

**Table 1.** Observation details, coordinates and radial velocities for our spectroscopic targets.

ID	spectrum	exp time [s]	Obs-date	airmass	RA	DEC	RV	RV <sub>helio</sub>
					J2000	J2000	[km s <sup>-1</sup> ]	[km s <sup>-1</sup> ]
NGC6934-n2	MIKE	2×1800	2017/05/05	~1.5	20:34:10.694	07:24:19.393	-433.37	-406.29
	GRACES	4×1050	2015/08/13	~1.1			-404.15	-407.93
NGC6934-a2	MIKE	2×1800	2017/05/05	~1.3	20:34:07.579	07:24:17.220	-427.70	-400.59
	GRACES	2×1000 - 2×1020	2015/12/15-16	~1.9			-380.23	-401.37
NGC6934-n1	GRACES	4×1010	2015-08-13	~1.3	20:34:10.399	07:24:17.964	-407.95	-411.89
NGC6934-a1	GRACES	2×1550	2015-12-18-22	~1.9	20:34:16.460	07:24:53.374	-382.42	-402.09

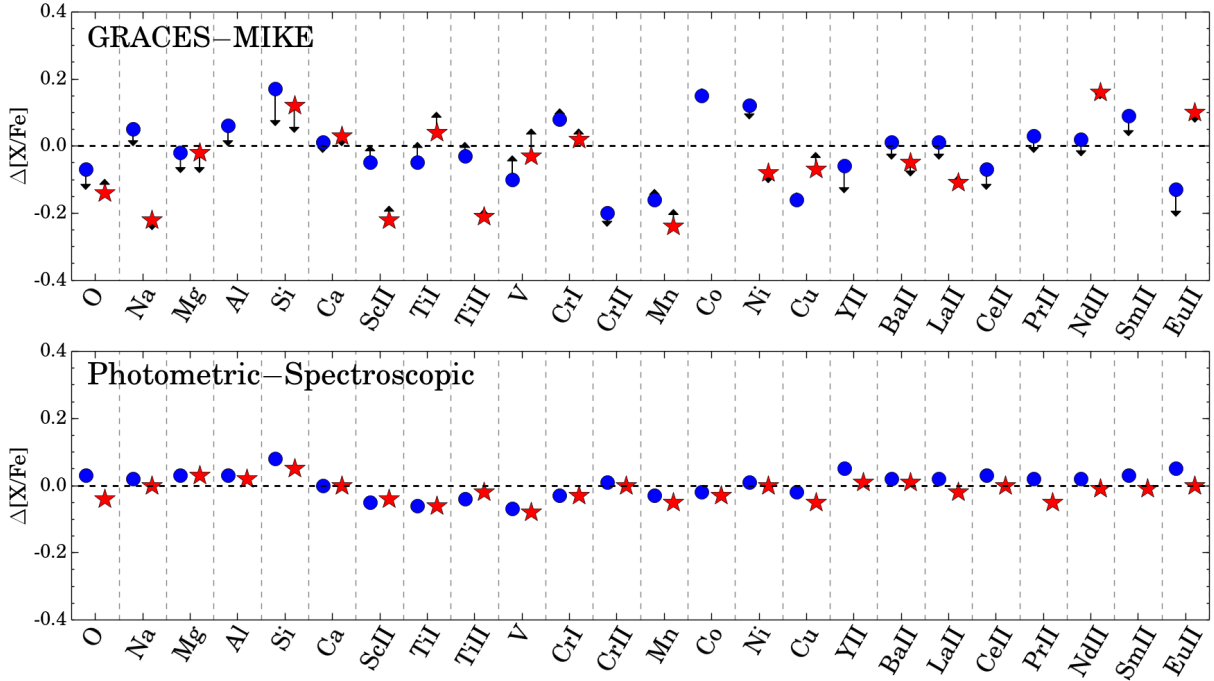


**Figure 3.** *Upper panel:* abundance ratio differences,  $[X/Fe]_{\text{GRACES}} - [X/Fe]_{\text{MIKE}}$ , obtained for the stars n2 (blue circle) and a2 (red star), observed with both the MIKE and GRACES spectrographs. *Lower panel:* abundance ratios differences,  $[X/Fe]_{\text{phot}} - [X/Fe]_{\text{spectr}}$ , derived for n2 and a2, observed with MIKE spectra, and analyzed by using stellar parameters from photometry ( $[X/Fe]_{\text{phot}}$ ) and spectral Fe lines ( $[X/Fe]_{\text{spectr}}$ ). The offsets ( $\Delta[X/Fe] = [X/Fe]_{\text{phot}} - [X/Fe]_{\text{spectr}}$ ) are shown in the upper panel with black arrows to visualize possible differences in the abundance ratios due to the different sets of atmospheric parameters assumed for MIKE and GRACES spectra.

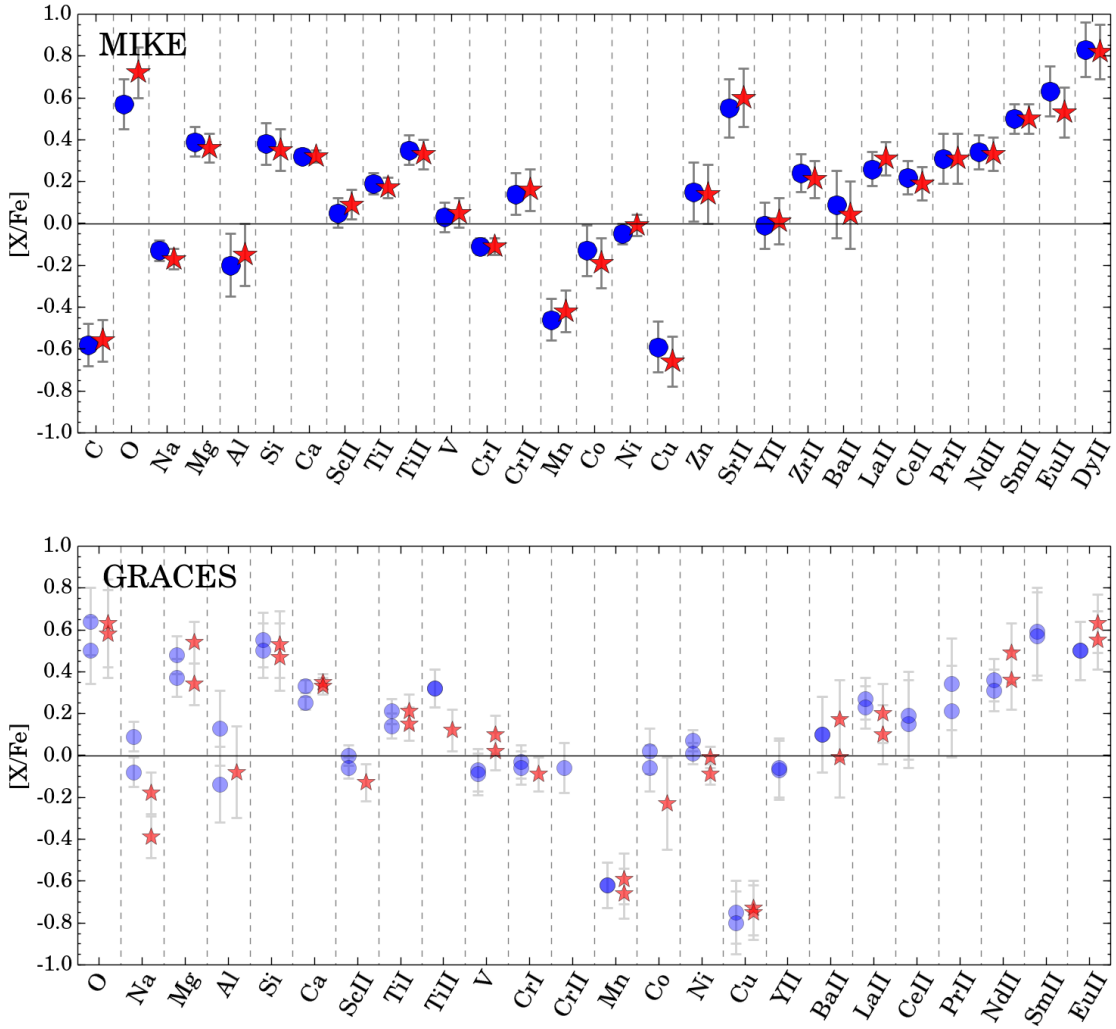


**Figure 4.** Summary of the abundance ratios results obtained from the MIKE (upper panel) and GRACES (lower panel) spectra. For each species, we plot the  $[X/Fe]$  relative abundances. In both panels, red star-like symbols are used for stars located on the red sequence of the chromosome map, while, filled blue circles are for stars on the *normal* sequence.





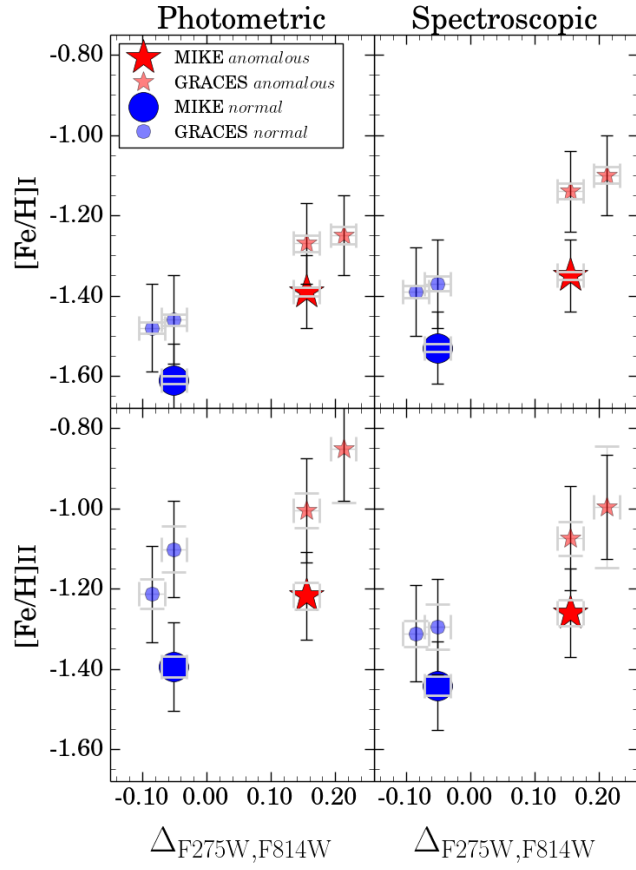


**Figure 6.** Chemical abundances obtained for Fe I and Fe II by using atmospheric parameters derived from Fe spectral lines (right panels) and from photometry (left panels). Stars in the *normal* and red sequence of the chromosome map have been plotted with blue circles and red starlike symbols, respectively. Results obtained from MIKE and GRACES have been distinguished by using larger darker symbols for MIKE, and smaller lighter symbols for GRACES.

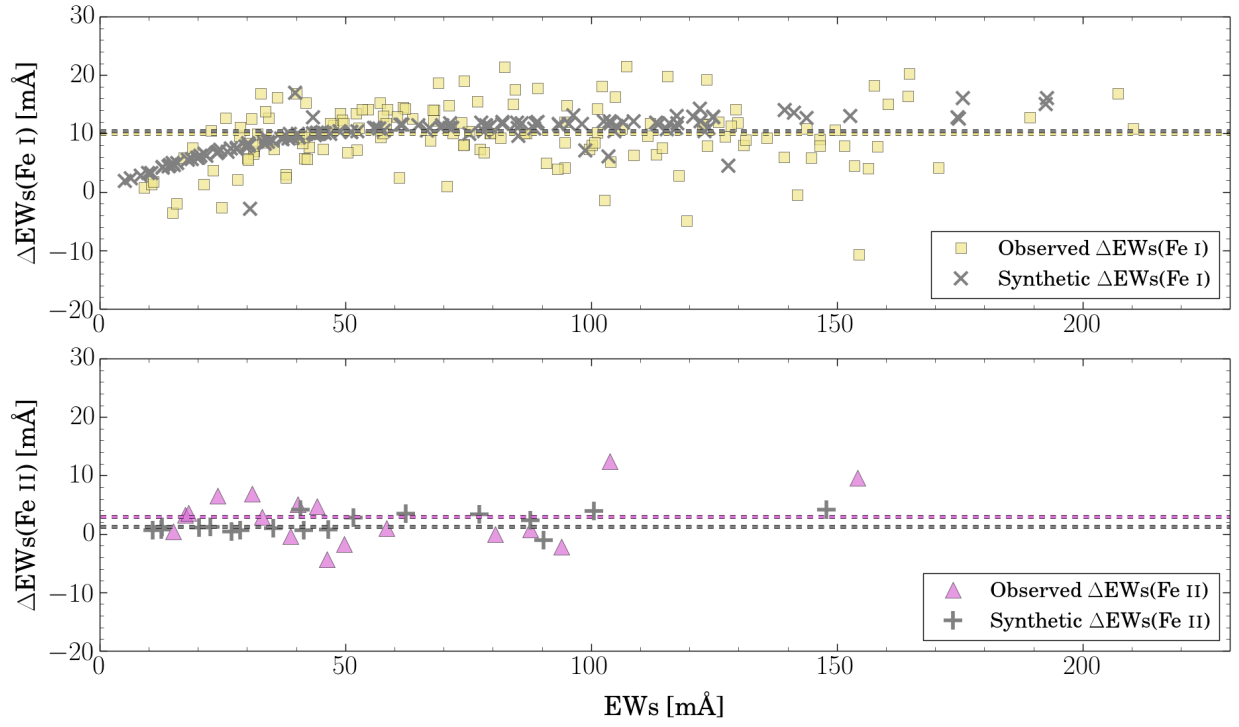


**Figure 7.** The observed difference in Fe I (upper panel, yellow squares) and Fe II (lower panel, magenta triangles) EWs between the stars n2 and a2, observed with MIKE, as a function of EW. The two stars have very similar atmospheric parameters, but have  $[\text{Fe}/\text{H}]$  differing by  $\sim 0.20$  dex. Grey symbols in both panels represent the EW differences for the same Fe lines, but computed from two synthetic spectra with the same atmospheric parameters as the two program stars and a difference of 0.2 dex in  $[\text{Fe}/\text{H}]$ .

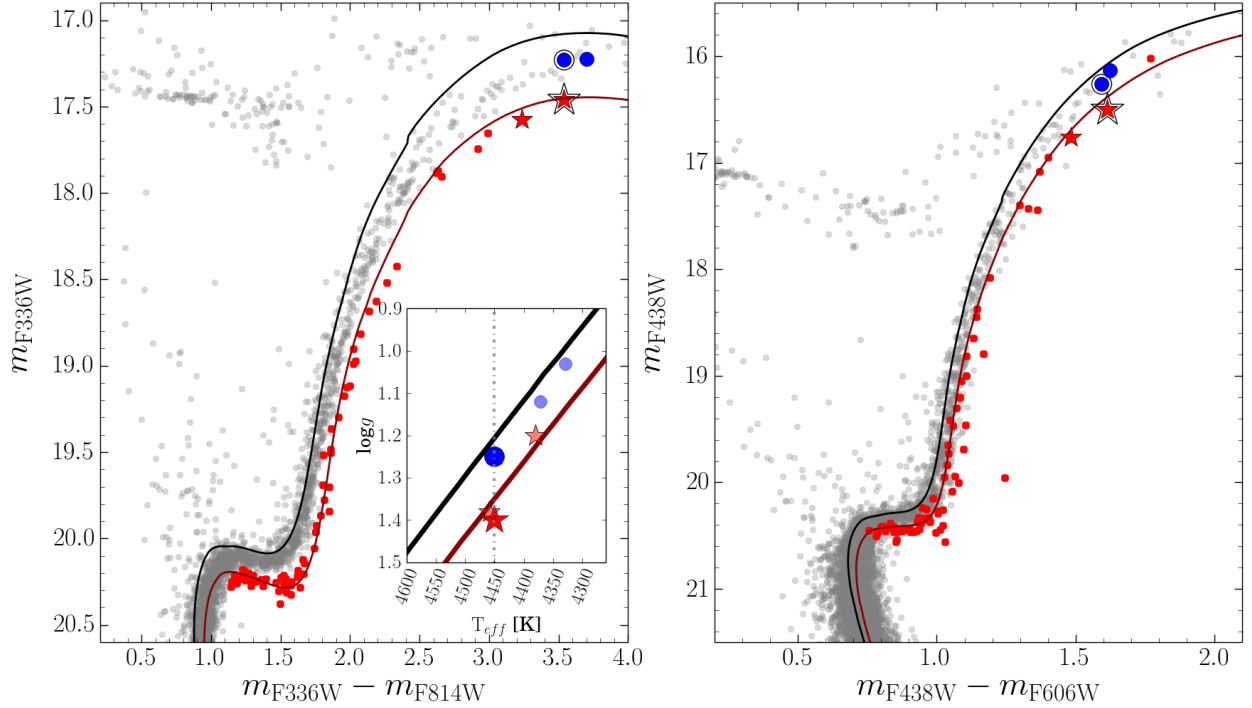


**Figure 8.**  $m_{F336W}$  versus  $m_{F336W} - m_{F814W}$  (left panel) and  $m_{F438W}$  versus  $m_{F438W} - m_{F606W}$  (right panel) CMDs for NGC 6934. *Anomalous* RGB stars and faint SGB stars have been plotted in red colours. Superimposed on the CMDs are two isochrones, from the Dartmouth database (Dotter et al. 2008), with the same age (12.25 Gyr), helium ( $Y=0.2471$ ) and  $\alpha$  content ( $[\alpha/Fe]=+0.40$ ), but different metallicity. Specifically, the black isochrone has  $[Fe/H]=-1.60$ , and the dark-red one  $[Fe/H]=-1.40$  dex. The inset on the left panel shows the  $\log g$  versus  $T_{\text{eff}}$  theoretical plane with the pattern corresponding to the two isochrones, together with the adopted stellar parameters for the target stars. The plotted  $\log g$ - $T_{\text{eff}}$  values have been derived spectroscopically for the MIKE data (plotted with larger symbols), and photometrically for GRACES data (plotted with smaller lighter symbols).

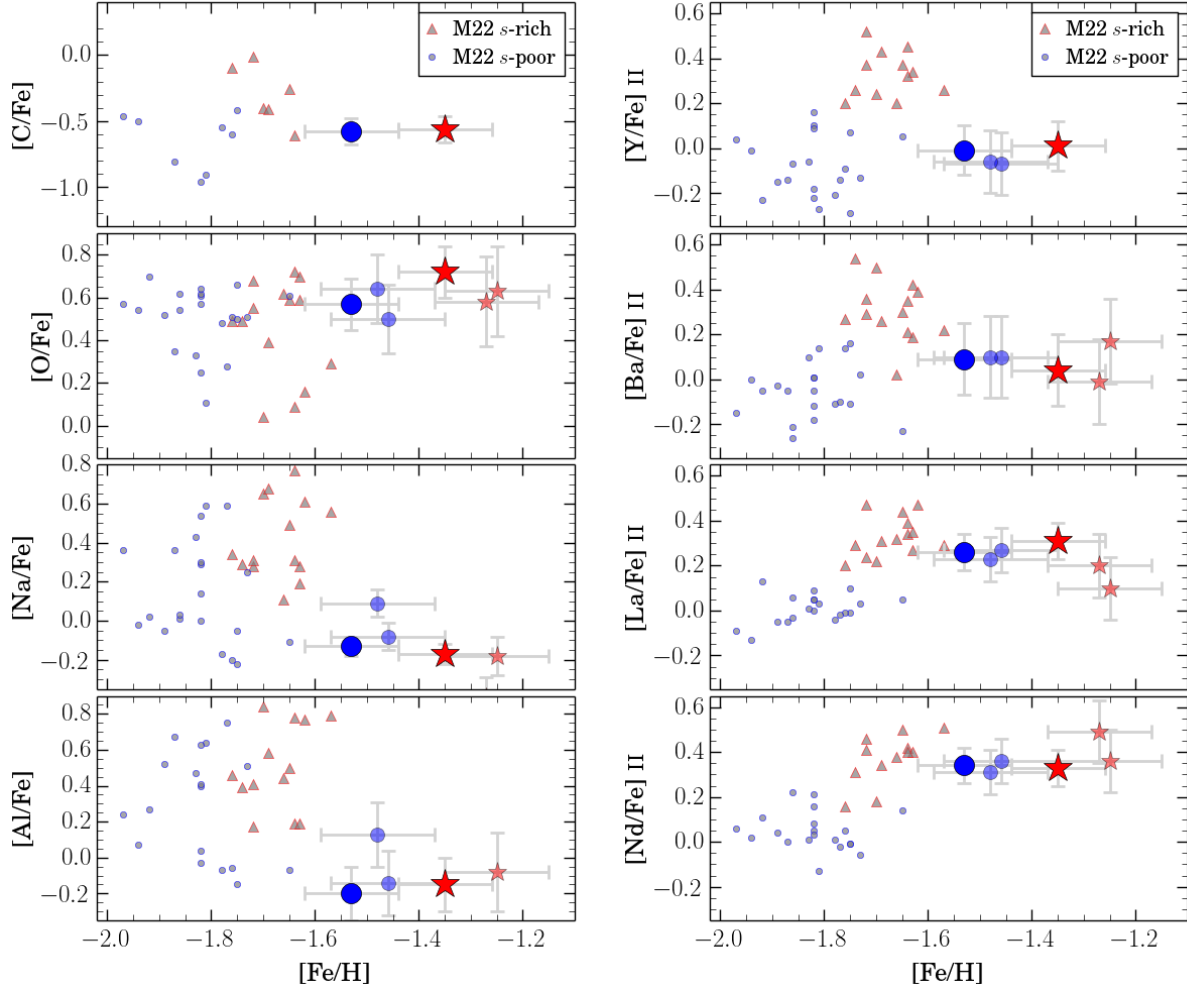


**Figure 9.** Abundance ratios of light elements [C-O-Na-Al/Fe] (left panel) and [Y-Ba-La-Nd/Fe] II (right panel), derived for NGC 6934 as function of [Fe/H], compared to the two  $s$  groups observed in M 22.  $s$ -poor and  $s$ -rich stars in M 22 are plotted with small grey-blue circles and grey-red triangles, respectively. Due to the different adopted O solar abundance, [O/Fe] abundances for M 22 have been shifted by +0.14 dex. Blue circles and red star-like symbols represent stars in the *normal* and red sequence of the NGC 6934 chromosome map, respectively.

**Table 2.** Atmospheric parameters, derived from spectroscopy and photometry, and corresponding Fe I and Fe II abundances (with the associated  $\sigma$  and number of spectral lines) for our targets. Results are listed for both MIKE and GRACES spectra.

ID	SOURCE	T <sub>eff</sub> (K)	log <i>g</i> (cgs)	[A/H] (dex)	$\xi_t$ (km s <sup>-1</sup> )	Spectroscopic				Photometric				$\sigma$					
						$\log \epsilon(\text{Fe I})$	$\sigma$	#	$\log \epsilon(\text{Fe II})$	$\sigma$	#	T <sub>eff</sub> (K)	log <i>g</i> (cgs)		[A/H] (dex)	$\xi_t$ (km s <sup>-1</sup> )	$\log \epsilon(\text{Fe I})$	$\sigma$	$\log \epsilon(\text{Fe II})$
NGC6934-n2	MIKE	4450	1.25	-1.53	1.78	5.968	0.122	153	6.058	0.097	17	4372	1.22	-1.61	1.78	5.886	0.126	6.1055	0.105
	GRACES	4500	1.10	-1.37	1.77	6.127	0.142	119	6.205	0.169	10	4372	1.22	-1.46	1.69	6.038	0.149	6.3985	0.172
NGC6934-a2	MIKE	4450	1.40	-1.35	1.80	6.143	0.128	157	6.240	0.133	18	4380	1.30	-1.39	1.75	6.096	0.128	6.282	0.141
	GRACES	4550	1.60	-1.14	2.00	6.361	0.196	106	6.425	0.113	8	4380	1.30	-1.27	1.90	6.231	0.204	6.494	0.114
NGC6934-n1	GRACES	4445	1.13	-1.39	1.95	6.108	0.141	112	6.188	0.101	11	4329	1.13	-1.48	1.88	6.019	0.146	6.287	0.114
NGC6934-a1	GRACES	4650	1.50	-1.10	1.97	6.399	0.165	65	6.504	0.262	4	4459	1.48	-1.25	1.85	6.252	0.178	6.648	0.230

**Table 3.** Line list with the measured EWs for the program stars observed with MIKE and GRACES. Only a portion of this table is shown here to demonstrate its form and content. A machine-readable version will be available.

Wavelength [Å]	Species	L.E.P. [eV]	$\log gf$	n2 EW <sub>MIKE</sub> [mÅ]	a2 EW <sub>MIKE</sub> [mÅ]	n2 EW <sub>GRACES</sub> [mÅ]	a2 EW <sub>GRACES</sub> [mÅ]	n1	a1
4139.94	FeI	0.99	-3.63	85.7	107.2	-	-	-	-
4439.89	FeI	2.28	-3.00	69.7	70.7	-	-	-	-
4445.48	FeI	0.09	-5.44	92.3	99.6	-	-	-	-
4489.75	FeI	0.12	-3.97	152.4	156.4	-	-	-	-
4574.23	FeI	3.21	-2.36	34.9	37.9	-	-	-	-
4602.01	FeI	1.61	-3.15	100.2	112.0	90.6	-	133.9	-
4602.95	FeI	1.49	-2.22	148.0	164.4	148.7	-	-	-
4658.30	FeI	3.27	-2.96	-	18.8	-	-	-	-
4788.76	FeI	3.24	-1.54	61.9	71.9	71.7	-	-	-
4839.55	FeI	3.27	-1.84	61.7	73.6	70.2	-	-	-
4859.74	FeI	2.87	-0.78	139.0	149.6	-	-	-	-
4885.43	FeI	3.88	-1.15	58.6	61.0	-	-	-	-
4917.24	FeI	4.19	-1.27	45.1	52.3	59.1	-	41.7	-
4924.77	FeI	2.28	-2.29	111.2	122.8	114.8	-	128.9	-

**Table 4.** Analysed chemical abundances from C to Ni.

ID	spectrum	[C/Fe]	$\sigma$	#	[O/Fe]	$\sigma$	#	[Na/Fe]	$\sigma$	[Na/Fe] <sub>NLTE</sub>	$\sigma$	#	[Mg/Fe]	$\sigma$	#	[Al/Fe]	$\sigma$	#
NGC6934-n2	MIKE	-0.58	0.02	2	0.57	0.01	2	0.05	0.24	-0.13	0.08	5	0.39	0.00	2	-0.20	0.13	2
	GRACES	-	-	-	0.50	0.08	2	0.08	0.31	-0.08	0.30	3	0.37	0.04	2	-0.14	0.17	2
NGC6934-a2	MIKE	-0.56	0.01	2	0.72	0.08	2	0.00	0.23	-0.17	0.07	6	0.36	0.00	2	-0.15	0.05	2
	GRACES	-	-	-	0.58	0.13	2	-0.27	0.28	-0.39	0.15	4	0.34	0.07	2	-	-	-
NGC6934-n1	GRACES	-	-	-	0.64	0.04	2	0.22	0.08	0.09	0.09	5	0.48	0.11	2	+0.13	0.02	2
NGC6934-a1	GRACES	-	-	-	0.63	0.13	2	0.17	-	-0.18	-	1	0.54	-	1	-0.08	-	1

ID	spectrum	[Si/Fe]	$\sigma$	#	[Ca/Fe]	$\sigma$	#	[Sc/Fe] <sub>II</sub>	$\sigma$	#	[Ti/Fe] <sub>I</sub>	$\sigma$	#	[Ti/Fe] <sub>II</sub>	$\sigma$	#
NGC6934-n2	MIKE	0.38	0.13	9	0.32	0.10	17	0.05	0.20	6	0.19	0.10	29	0.35	0.16	9
	GRACES	0.55	0.08	4	0.33	0.09	17	0.00	0.27	7	0.14	0.23	21	0.32	0.34	3
NGC6934-a2	MIKE	0.35	0.13	11	0.32	0.10	19	0.09	0.12	7	0.17	0.16	32	0.33	0.12	10
	GRACES	0.47	0.27	2	0.35	0.24	18	-0.13	0.35	4	0.21	0.16	16	0.12	0.18	2
NGC6934-n1	GRACES	0.50	0.04	4	0.25	0.12	16	-0.06	0.12	6	0.21	0.25	18	0.32	0.15	4
NGC6934-a1	GRACES	0.53	-	1	0.33	0.20	12	-	-	-	0.15	0.09	8	-	-	-

ID	spectrum	[V/Fe]	$\sigma$	#	[Cr/Fe] <sub>I</sub>	$\sigma$	#	[Cr/Fe] <sub>II</sub>	$\sigma$	#	[Mn/Fe]	$\sigma$	#	[Co/Fe]	$\sigma$	#	[Ni/Fe]	$\sigma$	#
NGC6934-n2	MIKE	0.03	0.11	14	-0.11	0.09	10	0.14	-	1	-0.46	0.13	9	-0.13	-	1	-0.05	0.14	24
	GRACES	-0.07	0.14	10	-0.03	0.17	8	-0.06	-	1	-0.62	0.15	9	0.02	-	1	+0.07	0.24	14
NGC6934-a2	MIKE	0.05	0.09	14	-0.11	0.09	10	0.16	0.24	2	-0.42	0.08	9	-0.19	0.09	2	-0.01	0.14	23
	GRACES	0.02	0.18	10	-0.09	0.38	5	-	-	-	-0.66	0.09	5	-	-	-	-0.09	0.14	14
NGC6934-n1	GRACES	-0.09	0.12	9	-0.06	0.30	4	-	-	-	-0.62	0.12	5	-0.06	-	1	+0.01	0.13	17
NGC6934-a1	GRACES	0.10	0.14	6	-	-	-	-	-	-	-0.59	0.14	5	-0.23	-	1	-0.01	0.16	7

**Table 5.** Analysed chemical abundances from Cu to Dy.

ID	spectrum	[Cu/Fe]	$\sigma$	#	[Zn/Fe]	$\sigma$	#	[Sr/Fe] II	$\sigma$	#	[Y/Fe] II	$\sigma$	#	[Zr/Fe] II	$\sigma$	#
NGC6934-n2	MIKE	-0.59	0.16	2	0.15	0.01	2	0.55	-	1	-0.01	0.02	4	0.24	-	1
	GRACES	-0.75	0.15	2	-	-	-	-	-	-	-0.07	0.17	4	-	-	-
NGC6934-a2	MIKE	-0.66	0.01	2	0.14	0.11	2	0.60	-	1	0.01	0.06	4	0.21	-	1
	GRACES	-0.73	-	1	-	-	-	-	-	-	-	-	-	-	-	-
NGC6934-n1	GRACES	-0.80	-	1	-	-	-	-	-	-	-0.06	0.10	2	-	-	-
NGC6934-a1	GRACES	-0.75	-	1	-	-	-	-	-	-	-	-	-	-	-	-

---

ID	spectrum	[Ba/Fe] II	$\sigma$	#	ID	spectrum	[La/Fe] II	$\sigma$	#	[Ce/Fe] II	$\sigma$	#	[Pr/Fe] II
NGC6934-n2	MIKE	0.09	0.09	3	0.26	0.09	8	0.22	0.07	7	0.31	0.03	2
	GRACES	0.10	0.05	3	0.27	0.13	6	0.15	-	1	0.34	-	1
NGC6934-a2	MIKE	0.04	0.05	3	0.31	0.08	8	0.19	0.09	7	0.31	0.13	2
	GRACES	-0.01	0.06	3	0.20	0.05	2	-	-	-	-	-	-
NGC6934-n1	GRACES	0.10	0.08	3	0.23	0.12	6	0.19	0.03	2	0.21	-	1
NGC6934-a1	GRACES	0.17	0.23	3	0.10	-	1	-	-	-	-	-	-

---

$\sigma$	#	[Nd/Fe] II	$\sigma$	#	[Sm/Fe] II	$\sigma$	#	[Eu/Fe] II	$\sigma$	#	[Dy/Fe] II	$\sigma$	#
NGC6934-n2	MIKE	0.34	0.09	18	0.50	0.07	14	0.63	-	1	0.83	-	1
	GRACES	0.36	0.09	10	0.59	0.17	3	0.50	-	1	-	-	-
NGC6934-a2	MIKE	0.33	0.14	18	0.50	0.13	14	0.53	-	1	0.82	-	1
	GRACES	0.49	0.05	3	-	-	-	0.63	-	1	-	-	-
NGC6934-n1	GRACES	0.31	0.11	11	0.57	0.25	4	0.50	-	1	-	-	-
NGC6934-a1	GRACES	0.36	0.04	3	-	-	-	0.55	-	1	-	-	-

**Table 6.** Sensitivity of the derived abundances to the uncertainties in atmospheric parameters and uncertainties due to the errors in the EWs measurements or in the  $\chi$ -square fitting procedure. We reported the total internal uncertainty ( $\sigma_{\text{total}}$ ) obtained by the quadratic sum of all the contributors to the error.

	$\Delta T_{\text{eff}}$	$\Delta \log g$	$\Delta \xi_t$	$\Delta [A/H]$	$\sigma_{\text{EWs/fit}}$	$\sigma_{\text{total}}$
	$\pm 50$ K	$\pm 0.20$	$\pm 0.20$ km s <sup>-1</sup>	$\pm 0.10$ dex		
	MIKE					
[C/Fe]	$\pm 0.07$	$\pm 0.00$	$\pm 0.00$	$\mp 0.03$	$\pm 0.06$	$\pm 0.10$
[O/Fe]	$\pm 0.00$	$\pm 0.07$	$\mp 0.00$	$\pm 0.03$	$\pm 0.09$	$\pm 0.12$
[Na/Fe]	$\mp 0.01$	$\mp 0.01$	$\pm 0.03$	$\mp 0.01$	$\pm 0.04$	$\pm 0.05$
[Mg/Fe]	$\mp 0.01$	$\mp 0.02$	$\mp 0.01$	$\pm 0.00$	$\pm 0.07$	$\pm 0.07$
[Al/Fe]	$\pm 0.05$	$\mp 0.00$	$\pm 0.01$	$\pm 0.00$	$\pm 0.14$	$\pm 0.15$
[Si/Fe]	$\mp 0.07$	$\pm 0.01$	$\pm 0.06$	$\pm 0.02$	$\pm 0.03$	$\pm 0.10$
[Ca/Fe]	$\pm 0.00$	$\mp 0.01$	$\mp 0.01$	$\mp 0.01$	$\pm 0.02$	$\pm 0.03$
[Sc/Fe] II	$\pm 0.05$	$\mp 0.00$	$\pm 0.02$	$\mp 0.00$	$\pm 0.04$	$\pm 0.07$
[Ti/Fe] I	$\pm 0.04$	$\mp 0.01$	$\pm 0.01$	$\mp 0.02$	$\pm 0.02$	$\pm 0.05$
[Ti/Fe] II	$\pm 0.04$	$\mp 0.01$	$\mp 0.04$	$\mp 0.01$	$\pm 0.03$	$\pm 0.07$
[V/Fe]	$\pm 0.05$	$\mp 0.00$	$\pm 0.04$	$\mp 0.01$	$\pm 0.02$	$\pm 0.07$
[Cr/Fe] I	$\pm 0.03$	$\mp 0.01$	$\mp 0.00$	$\mp 0.01$	$\pm 0.03$	$\pm 0.04$
[Cr/Fe] II	$\pm 0.00$	$\mp 0.00$	$\pm 0.02$	$\mp 0.01$	$\pm 0.10$	$\pm 0.10$
[Mn/Fe]	$\pm 0.08$	$\pm 0.00$	$\mp 0.02$	$\mp 0.02$	$\pm 0.05$	$\pm 0.10$
[Fe/H] I	$\pm 0.06$	$\pm 0.00$	$\mp 0.07$	$\mp 0.00$	$\pm 0.01$	$\pm 0.09$
[Fe/H] II	$\mp 0.05$	$\pm 0.07$	$\mp 0.06$	$\pm 0.04$	$\pm 0.03$	$\pm 0.11$
[Co/Fe]	$\pm 0.00$	$\pm 0.00$	$\pm 0.06$	$\pm 0.01$	$\pm 0.10$	$\pm 0.12$

Table 6 continued on next page

**Table 6** (*continued*)

	$\Delta T_{\text{eff}}$	$\Delta \log g$	$\Delta \xi_t$	$\Delta [A/H]$	$\sigma_{\text{EWs/fit}}$	$\sigma_{\text{total}}$
	$\pm 50 \text{ K}$	$\pm 0.20$	$\pm 0.20 \text{ km s}^{-1}$	$\pm 0.10 \text{ dex}$		
[Ni/Fe]	$\mp 0.01$	$\pm 0.01$	$\pm 0.04$	$\pm 0.01$	$\pm 0.02$	$\pm 0.05$
[Cu/Fe]	$\pm 0.08$	$\mp 0.00$	$\mp 0.07$	$\pm 0.00$	$\mp 0.06$	$\pm 0.12$
[Zn/Fe]	$\mp 0.10$	$\pm 0.03$	$\pm 0.01$	$\pm 0.03$	$\pm 0.08$	$\pm 0.14$
[Sr/Fe] II	$\pm 0.09$	$\mp 0.01$	$\mp 0.06$	$\mp 0.03$	$\pm 0.08$	$\pm 0.14$
[Y/Fe] II	$\pm 0.00$	$\pm 0.05$	$\mp 0.09$	$\pm 0.00$	$\pm 0.04$	$\pm 0.11$
[Zr/Fe] II	$\pm 0.02$	$\pm 0.06$	$\mp 0.02$	$\pm 0.01$	$\pm 0.06$	$\pm 0.09$
[Ba/Fe] II	$\pm 0.01$	$\pm 0.07$	$\mp 0.13$	$\pm 0.03$	$\pm 0.04$	$\pm 0.16$
[La/Fe] II	$\pm 0.01$	$\pm 0.07$	$\mp 0.02$	$\pm 0.03$	$\pm 0.03$	$\pm 0.08$
[Ce/Fe] II	$\pm 0.00$	$\pm 0.05$	$\mp 0.05$	$\pm 0.02$	$\pm 0.04$	$\pm 0.08$
[Pr/Fe] II	$\pm 0.00$	$\pm 0.06$	$\pm 0.00$	$\pm 0.04$	$\pm 0.09$	$\pm 0.12$
[Nd/Fe] II	$\pm 0.02$	$\pm 0.06$	$\mp 0.04$	$\pm 0.01$	$\pm 0.02$	$\pm 0.08$
[Sm/Fe] II	$\pm 0.01$	$\pm 0.06$	$\mp 0.03$	$\pm 0.01$	$\pm 0.02$	$\pm 0.07$
[Eu/Fe] II	$\mp 0.01$	$\pm 0.07$	$\pm 0.00$	$\pm 0.04$	$\pm 0.09$	$\pm 0.12$
[Dy/Fe] II	$\pm 0.03$	$\pm 0.08$	$\mp 0.06$	$\mp 0.01$	$\pm 0.08$	$\pm 0.13$
GRACES <i>normal stars</i>						
[O/Fe]	$\pm 0.01$	$\pm 0.07$	$\pm 0.00$	$\pm 0.04$	$\pm 0.14$	$\pm 0.16$
[Na/Fe]	$\mp 0.01$	$\mp 0.02$	$\pm 0.04$	$\mp 0.01$	$\pm 0.05$	$\pm 0.07$
[Mg/Fe]	$\mp 0.01$	$\mp 0.03$	$\pm 0.01$	$\mp 0.00$	$\pm 0.08$	$\pm 0.09$
[Al/Fe]	$\pm 0.03$	$\mp 0.00$	$\pm 0.00$	$\pm 0.00$	$\pm 0.18$	$\pm 0.18$
[Si/Fe]	$\mp 0.09$	$\pm 0.01$	$\pm 0.06$	$\pm 0.02$	$\pm 0.06$	$\pm 0.13$
[Ca/Fe]	$\pm 0.00$	$\mp 0.02$	$\mp 0.01$	$\mp 0.01$	$\pm 0.02$	$\pm 0.03$
[Sc/Fe] II	$\pm 0.01$	$\mp 0.00$	$\pm 0.00$	$\mp 0.02$	$\pm 0.04$	$\pm 0.05$
[Ti/Fe] I	$\pm 0.05$	$\mp 0.01$	$\pm 0.00$	$\mp 0.02$	$\pm 0.02$	$\pm 0.06$
[Ti/Fe] II	$\pm 0.01$	$\mp 0.01$	$\mp 0.06$	$\mp 0.02$	$\pm 0.06$	$\pm 0.09$
[V/Fe]	$\pm 0.07$	$\mp 0.00$	$\pm 0.07$	$\mp 0.01$	$\pm 0.03$	$\pm 0.10$
[Cr/Fe] I	$\pm 0.05$	$\mp 0.01$	$\mp 0.04$	$\mp 0.02$	$\pm 0.04$	$\pm 0.08$
[Cr/Fe] II	$\mp 0.02$	$\mp 0.00$	$\pm 0.03$	$\mp 0.02$	$\pm 0.11$	$\pm 0.12$
[Mn/Fe]	$\pm 0.09$	$\mp 0.00$	$\mp 0.02$	$\mp 0.02$	$\pm 0.05$	$\pm 0.11$
[Fe/H] I	$\pm 0.06$	$\pm 0.00$	$\mp 0.09$	$\pm 0.00$	$\pm 0.01$	$\pm 0.11$
[Fe/H] II	$\mp 0.04$	$\pm 0.06$	$\mp 0.07$	$\pm 0.05$	$\pm 0.04$	$\pm 0.12$
[Co/Fe]	$\pm 0.01$	$\pm 0.00$	$\pm 0.07$	$\pm 0.01$	$\pm 0.09$	$\pm 0.11$
[Ni/Fe]	$\mp 0.01$	$\pm 0.01$	$\pm 0.03$	$\pm 0.01$	$\pm 0.03$	$\pm 0.05$
[Cu/Fe]	$\pm 0.10$	$\pm 0.00$	$\mp 0.07$	$\mp 0.02$	$\pm 0.09$	$\pm 0.15$
[Y/Fe] II	$\pm 0.02$	$\pm 0.04$	$\mp 0.08$	$\mp 0.01$	$\pm 0.11$	$\pm 0.14$
[Ba/Fe] II	$\pm 0.01$	$\pm 0.07$	$\mp 0.15$	$\pm 0.04$	$\pm 0.07$	$\pm 0.18$
[La/Fe] II	$\pm 0.01$	$\pm 0.06$	$\mp 0.01$	$\pm 0.04$	$\pm 0.07$	$\pm 0.10$
[Ce/Fe] II	$\mp 0.02$	$\pm 0.04$	$\mp 0.06$	$\pm 0.02$	$\pm 0.20$	$\pm 0.21$
[Pr/Fe] II	$\pm 0.00$	$\pm 0.08$	$\pm 0.00$	$\pm 0.04$	$\pm 0.20$	$\pm 0.22$
[Nd/Fe] II	$\pm 0.00$	$\pm 0.06$	$\mp 0.04$	$\pm 0.02$	$\pm 0.06$	$\pm 0.10$
[Sm/Fe] II	$\mp 0.01$	$\pm 0.03$	$\mp 0.05$	$\pm 0.00$	$\pm 0.20$	$\pm 0.21$

*Table 6 continued on next page*



**Table 6** (*continued*)

	$\Delta T_{\text{eff}}$	$\Delta \log g$	$\Delta \xi_t$	$\Delta [A/H]$	$\sigma_{\text{EWs/fit}}$	$\sigma_{\text{total}}$
	$\pm 50 \text{ K}$	$\pm 0.20$	$\pm 0.20 \text{ km s}^{-1}$	$\pm 0.10 \text{ dex}$		
[Eu/Fe] II	$\pm 0.00$	$\pm 0.08$	$\pm 0.00$	$\pm 0.05$	$\pm 0.10$	$\pm 0.14$
GRACES <i>anomalous</i> stars						
[O/Fe]	$\pm 0.00$	$\pm 0.06$	$\pm 0.00$	$\pm 0.05$	$\pm 0.20$	$\pm 0.21$
[Na/Fe]	$\mp 0.00$	$\mp 0.01$	$\pm 0.06$	$\mp 0.01$	$\pm 0.08$	$\pm 0.10$
[Mg/Fe]	$\mp 0.01$	$\mp 0.03$	$\pm 0.00$	$\mp 0.01$	$\pm 0.09$	$\pm 0.10$
[Al/Fe]	$\pm 0.03$	$\mp 0.00$	$\pm 0.01$	$\mp 0.01$	$\pm 0.22$	$\pm 0.22$
[Si/Fe]	$\mp 0.08$	$\pm 0.01$	$\pm 0.06$	$\pm 0.02$	$\pm 0.12$	$\pm 0.16$
[Ca/Fe]	$\pm 0.02$	$\mp 0.01$	$\mp 0.01$	$\mp 0.02$	$\pm 0.03$	$\pm 0.04$
[Sc/Fe] II	$\pm 0.05$	$\mp 0.00$	$\pm 0.00$	$\mp 0.01$	$\pm 0.07$	$\pm 0.09$
[Ti/Fe] I	$\pm 0.06$	$\pm 0.00$	$\pm 0.03$	$\mp 0.02$	$\pm 0.03$	$\pm 0.08$
[Ti/Fe] II	$\pm 0.06$	$\mp 0.00$	$\mp 0.05$	$\mp 0.01$	$\pm 0.06$	$\pm 0.10$
[V/Fe]	$\pm 0.06$	$\mp 0.00$	$\pm 0.05$	$\mp 0.02$	$\pm 0.03$	$\pm 0.09$
[Cr/Fe] I	$\pm 0.05$	$\mp 0.00$	$\pm 0.00$	$\mp 0.02$	$\pm 0.06$	$\pm 0.08$
[Mn/Fe]	$\pm 0.10$	$\pm 0.00$	$\mp 0.01$	$\mp 0.02$	$\pm 0.06$	$\pm 0.12$
[Fe/H] I	$\pm 0.05$	$\pm 0.00$	$\mp 0.09$	$\pm 0.01$	$\pm 0.01$	$\pm 0.10$
[Fe/H] II	$\mp 0.08$	$\pm 0.06$	$\mp 0.06$	$\pm 0.04$	$\pm 0.05$	$\pm 0.13$
[Co/Fe]	$\mp 0.05$	$\mp 0.00$	$\pm 0.09$	$\mp 0.01$	$\pm 0.20$	$\pm 0.22$
[Ni/Fe]	$\mp 0.00$	$\pm 0.01$	$\pm 0.04$	$\pm 0.02$	$\pm 0.03$	$\pm 0.05$
[Cu/Fe]	$\pm 0.05$	$\pm 0.01$	$\mp 0.01$	$\mp 0.01$	$\pm 0.12$	$\pm 0.13$
[Ba/Fe] II	$\pm 0.01$	$\pm 0.06$	$\mp 0.15$	$\pm 0.03$	$\pm 0.10$	$\pm 0.19$
[La/Fe] II	$\pm 0.01$	$\pm 0.07$	$\pm 0.00$	$\pm 0.04$	$\pm 0.12$	$\pm 0.14$
[Nd/Fe] II	$\pm 0.01$	$\pm 0.06$	$\mp 0.06$	$\pm 0.04$	$\pm 0.11$	$\pm 0.14$
[Eu/Fe] II	$\mp 0.02$	$\pm 0.05$	$\pm 0.00$	$\pm 0.02$	$\pm 0.13$	$\pm 0.14$

**Table 7.** List of GCs with confirmed chemical and/or photometric anomalies. The listed chemical properties, as measured from spectroscopic data, include: (i) star-to-star variations in Fe, (ii) *s*-process elements, (iii) multiple *p*-capture (anti-)correlation (e.g. within groups of stars with different Fe and *s*-elements as displayed in Fig. 14 in Marino et al. 2011), (iv) differences in the overall C+N+O. For each GC we list a “Proposed Class”, which refers to the presence of variations in Fe (Iron-II), in *s*-elements (*s*-II), and multiple sequence on the chromosome map, as found in Milone et al. (2017, Type II). Further details in Section 6.

GC	CHEMICAL ABUNDANCE VARIATIONS							Proposed Class	
	metallicity	Literature	<i>s</i> -elements	Literature	<i>p</i> -capture elements in each Fe group	Literature	C+N+O		Literature
NGC1261	(?)		(?)		(?)	(?)		(?)	Type II
NGC1851	possible small	Carretta+10 Gratton+13 Marino+14	yes	YG08 <sup>a</sup> ; Villanova+10	yes	Carretta+10; Villanova+10	yes	Yong+14	Iron-II/ <i>s</i> -II/Type II
NGC362	(?)		yes	Carretta+13	(?)		(?)		<i>s</i> -II/Type II
NGC5139 ( $\omega$ Centauri)	yes	Norris+96; SK96 <sup>d</sup>	yes	NDaC95 <sup>b</sup> ; Smith+00; JP10 <sup>e</sup> ; Marino+11b; D’Orazi+11	yes	JP10 <sup>e</sup> ; Marino+11b	yes	Marino+12b	Iron-II/ <i>s</i> -II/Type II
NGC5286	yes	Marino+15	yes	Marino+15	yes	Marino+15	not-studied		Iron-II/ <i>s</i> -II/Type II
NGC5824	yes(?)	Da Costa+14	yes(?)	Roederer+16	not-studied		not-studied		Iron-II(?)/ <i>s</i> -II(?)
NGC6229	possible small	Johnson+17	yes	Johnson+17	no(?)	Johnson+17	not-studied		Iron-II(?)/ <i>s</i> -II
NGC6273 (M19)	yes	Johnson+15	yes	Johnson+15	yes	Johnson+15	not-studied		Iron-II/ <i>s</i> -II
NGC6388	(?)		(?)		(?)		(?)		Type II
NGC6656 (M22)	yes	Marino+09; Da Costa+09	yes	Marino+09,11a,12a	yes	Marino+09,11a	yes	Marino+11a Alves Brito+12	Iron-II/ <i>s</i> -II/Type II
NGC6715 (M54)	yes	Carretta+10	yes(?)	BWG99 <sup>e</sup>	yes	Carretta+10	not-studied		Iron II/ <i>s</i> -II(?)/Type II
NGC6934	yes	This work	no	This work	not-studied		not-studied		Iron II/ <i>s</i> -I/Type II
NGC7089 (M2)	yes	Yong+14	yes	Lardo+13; Yong+14	yes	Yong+14	not-studied		Iron-II/ <i>s</i> -II/Type II
Terzan 5	yes	Ferraro+09 Origlia+11 Massari+14	not studied		not studied		not-studied		Iron-II

<sup>a</sup>Yong & Grundahl (2008)

<sup>b</sup>Norris & Da Costa (1995)

<sup>c</sup>Johnson & Pilachowski (2010)

<sup>d</sup>Stuntz & Kraft (1996)

<sup>e</sup>Brown, Wallerstein & Gonzalez (1999)